ICARUS **124,** 62–85 (1996)
ARTICLE NO. 0190

Formation of the Giant Planets by Concurrent Accretion of Solids and Gas[1]

JAMES B. POLLACK[2]

Space Science Division, NASA Ames Research Center, Moffett Field, California 94035

OLENKA HUBICKYJ[3] AND PETER BODENHEIMER

UCO/Lick Observatory, University of California, Santa Cruz, California 95064
E-mail: peter@helios.ucsc.edu

JACK J. LISSAUER

Astronomy Program, Department of Earth and Space Sciences, State University of New York, Stony Brook, New York 11794

AND

MORRIS PODOLAK AND YUVAL GREENZWEIG

Department of Geophysics and Planetary Sciences, Tel Aviv University, Ramat Aviv, Israel, 69978

Received August 28, 1995; revised March 28, 1996

New numerical simulations of the formation of the giant planets are presented, in which for the first time both the gas and planetesimal accretion rates are calculated in a self-consistent, interactive fashion. The simulations combine three elements: (1) three-body accretion cross sections of solids onto an isolated planetary embryo, (2) a stellar evolution code for the planet's gaseous envelope, and (3) a planetesimal dissolution code within the envelope, used to evaluate the planet's effective capture radius and the energy deposition profile of accreted material. Major assumptions include: The planet is embedded in a disk of gas and small planetesimals with locally uniform initial surface mass density, and planetesimals are not allowed to migrate into or out of the planet's feeding zone.

All simulations are characterized by three major phases. During the first phase, the planet's mass consists primarily of solid material. The planetesimal accretion rate, which dominates that of gas, rapidly increases owing to runaway accretion, then decreases as the planet's feeding zone is depleted. During the second phase, both solid and gas accretion rates are small and nearly independent of time. The third phase, marked by runaway gas accretion, starts when the solid and gas masses are about equal. It is engendered by a strong positive feedback on the gas accretion rates, driven by the rapid contraction of the gaseous envelope and the rapid expansion of the outer boundary, which depends on the planet's total mass. The overall evolutionary time scale is generally determined by the length of the second phase.

The actual rates at which the giant planets accreted small planetesimals is probably intermediate between the constant rates assumed in most previous studies and the highly variable rates used here. Within the context of the adopted model of planetesimal accretion, the joint constraints of the time scale for dissipation of the solar nebula and the current high-Z masses of the giant planets lead to estimates of the initial surface density ($\sigma_{\rm init}$) of planetesimals in the outer region of the solar nebula. The results show that $\sigma_{\rm init} \approx 10$ g cm^{-2} near Jupiter's orbit and that $\sigma_{\rm init} \propto a^{-2}$, where a is the distance from the Sun. These values are a factor of 3 to 4 times as high as that of the "minimum-mass" solar nebula at Jupiter's distance and a factor of 2 to 3 times as high at Saturn's distance. The estimates for the formation time of Jupiter and Saturn are 1 to 10 million years, whereas those for Uranus fall in the range 2 to 16 million years. These estimates follow from the properties of our Solar System and do not necessarily apply to giant planets in other planetary systems.

1. INTRODUCTION

Unlike the terrestrial planets, the giant planets formed from significant quantities of both the gas and the solid material of the solar nebula. However, the giant planets are not made of solar proportions of the elements. Rather, all four giant planets preferentially accreted refractory ma-

[1] UCO/Lick Observatory Bulletin No. 1341.
[2] Deceased.
[3] Present address: SETI Institute, 2035 Landings Dr., Mountain View, CA 94043.

0019-1035/96 $18.00

terials, with the degree of enhancement, with respect to the Sun, varying progressively from a factor on the order of 5 for Jupiter to about 25 for Saturn to very roughly 300 for Uranus and Neptune (e.g., Pollack and Bodenheimer 1989, Podolak *et al.* 1993). Thus, it seems likely that the formation of the giant planets involved the ''binary'' accretion of solid planetesimals, the same process by which the terrestrial planets formed (Safronov 1969). However, unlike the terrestrial planets, the giant planets grew massive enough to capture large quantities of gas from the solar nebula.

Mizuno *et al.* (1978) and Mizuno (1980) were the first to show that the above conceptual model was able to account approximately for the relative amounts of high- and low-Z materials in the giant planets. We refer to the gaseous component, which is primarily H_2 and He, as the ''low-Z'' material, where Z indicates the atomic number. We refer to the solid material, which includes ''rock,'' ''CHON,'' and ''ice,'' as the ''high-Z'' material, even though ''ice'' and ''CHON'' include significant amounts of H. In particular, Mizuno and collaborators constructed a series of equilibrium model planets having solid (high-Z) cores and gaseous envelopes that joined smoothly with the solar nebula at their tidal radii. The models had low-Z envelopes that grew exponentially with increasing core mass, the two masses becoming approximately equal when the core mass reached a ''critical value'' of $M_{\rm crit} \sim 10\ M_\oplus$. Mizuno was unable to construct equilibrium models for larger envelope masses, which led him to suggest that the giant planets underwent a hydrodynamical collapse when their core masses exceeded $M_{\rm crit}$. Gas would have accreted very rapidly during this phase. The value of $M_{\rm crit}$ was found to depend very insensitively on the nebula boundary conditions and weakly on the amount of grain opacity assumed to be present in the outer portions of the envelope. Thus, this ''core instability'' model appeared capable of explaining why the high-Z masses of the giant planets were rather similar and had values on the order of 10 to $30 M_\oplus$.

Bodenheimer and Pollack (1986, hereafter referred to as BP86) carried out the first evolutionary calculation of the core instability model. They constructed sequences of quasi-hydrostatic models that were connected in time by a prescribed rate of solid-body accretion and whose envelopes evolved in time due to gas accretion and radiation to space. They assumed that the solid-body accretion rate was time invariant for a given evolutionary sequence, although this rate was varied among the different sequences. In these simulations, the rate of gas accretion exceeded the rate of planetesimal accretion by an amount that grew exponentially with time once the core mass was sufficiently massive. Since this mass is not precisely determined by the simulations (the transition is fairly rapid, but not abrupt) and it corresponds approximately to the point where the high-Z and the low-Z masses are equal, it will be referred to as the ''crossover mass'' ($M_{\rm cross}$) in the remainder of this paper. During this ''runaway'' gas accretion phase, the envelope did not undergo a hydrodynamic collapse as long as the solar nebula could supply gas rapidly enough to compensate for an increasingly rapid contraction of the outer envelope and an increasingly rapid expansion of the planet's sphere of influence. BP86 obtained a value of $M_{\rm cross}$ (which they referred to as the critical core mass in analogy with Mizuno)—about 10 to $30 M_\oplus$—somewhat larger than the values of $M_{\rm crit}$ obtained by Mizuno (1980). The values of $M_{\rm cross}$ were found to be very insensitive to the boundary conditions with the solar nebula, in accord with Mizuno's (1980) values for $M_{\rm crit}$; to be even more insensitive to the amount of grain opacity assumed in the outer envelope than Mizuno had found (due to the inclusion of water vapor opacity); and to have a mild sensitivity to the core accretion rate, with larger core accretion rates leading to a larger $M_{\rm cross}$. Thus, one could speculate that the modest variation in high-Z masses among the giant planets reflected variations in their rates of planetesimal accretion.

Pollack *et al.* (1986) and Podolak *et al.* (1988) examined the ability of accreted planetesimals to pass through the envelopes of the giant planets and reach the core intact. Using the model envelopes of BP86, they found that a combination of gas drag, evaporation, and dynamical pressure made it increasingly difficult for planetesimals to arrive intact at the core boundary once the envelope mass exceeds a few percent of $M_\oplus$. Thus, a significant fraction of the planetesimals accreted by the giant planets should have been dissolved in their envelopes, enriching them in high-Z elements. Such a scenario is able to account in an approximate way for the observed enhancement (with respect to solar values) of some high-Z elements in the atmospheres of the current giant planets and for the progressive enrichment of these elements from Jupiter to Saturn to Uranus/Neptune (Podolak *et al.* 1988, Simonelli *et al.* 1989).

Thus, it might appear that the core instability model is capable of explaining both the bulk mass properties and the atmospheric compositions of the giant planets. However, this model faces several potentially very important problems. First, Uranus and Neptune do not fit nicely into this picture. Their low-Z masses equal only about 10 to 20% of their high-Z masses. Thus, they would not have been expected to have attained $M_{\rm cross}$ before their accretion was halted. It is not obvious why their high-Z masses should be similar to those of Jupiter and Saturn. Furthermore, the period during which accreting giant planets have low- and high-Z masses similar to those of Uranus and Neptune represents only a tiny fraction of their total accretion time in the calculations of BP86. While one could postulate that the solar nebula vanished at just the right time to account for one of these planets, the a priori probability that planets

with the properties of Uranus and Neptune would be found in the same system would be incredibly small in this scenario.

The core instability scenario has been further analyzed by Wuchterl (1991), who used a radiation-hydrodynamics code rather than a quasi-static one. He finds that once the envelope mass has become comparable to the core mass, a dynamical instability develops that results in the ejection of much of the envelope, leaving a planet with a low-mass envelope and properties similar to those of Uranus and Neptune. The model does not account for the formation of Jupiter and Saturn, a problem that has not yet been resolved. Tajima and Nakagawa (preprint) have reexamined the evolution with the same assumptions as those of BP86 but with an independent code and have used a linear stability analysis to examine the properties of the envelope at all times. They find that the envelope is dynamically stable for all masses up to that of Jupiter, and that therefore the quasi-static approximation is justified. Nevertheless, Wuchterl (1995) continues to find dynamical instability unless the solar nebular density, $\rho_{\rm neb}$, is increased to 10^{-9} g cm^{-3} or higher (an order of magnitude higher than the standard value at Jupiter's distance), in which case he finds stable accretion to high envelope masses.

Another possible problem with the core instability hypothesis is that it does not account for the observed partitioning of high-Z material between a truly segregated inner core and the envelope. Recent interior models of the giant planets suggest that the cores of Jupiter and Saturn contain only a few $M_\oplus$, with the vast majority of the high-Z material residing in the envelopes (Zharkov and Gudkova 1991, Chabrier *et al.* 1992). Consequently, previous calculations that have implicitly assumed that planetesimals reach the core intact (e.g., Mizuno 1980, BP86) may not be directly relevant for estimating the mass of solids that needs to be accreted before runaway gas accretion takes place. In particular, these models probably overestimate the energy released by planetesimal accretion and thereby artificially delay the onset of rapid envelope contraction.

Finally, there is a possible problem with the accretion time scale. In his classical calculations of planetesimal accretion, Safronov (1969) obtained accretion time scales for Neptune that exceeded the age of the Solar System. A previous approach to the time scale problem was that of Stevenson (1984; see also Lissauer *et al.* 1995), who considered a core of the mass of Ganymede, from which icy material evaporated, forming a dense H_2O–H_2 envelope which had a relatively small value of $M_{\rm cross}$. However, other calculations suggest that this problem may be alleviated by some or all of the following factors: (1) rapid "runaway" accretion of solids by the largest planetary embryos (Levin 1978, Greenberg *et al.* 1978); (2) the possibility that the mass density of planetesimals in the giant planet region of the solar nebula exceeded somewhat the values given by the so-called "minimum mass" solar nebula (Lissauer 1987); (3) more rapid accretion times found in multiple zone simulations of planetesimal accretion by Wetherill (see, e.g., Lissauer *et al.* 1995). These points also suggest the real possibility that the rate of planetesimal accretion may have deviated by wide margins from a time-invariant value, especially in the case when a single dominant mass is present (Lissauer 1987).

In this paper, we improve the core instability model by constructing evolutionary models of the formation of the giant planets that allow for the interactions of planetesimals with the envelopes of the giant planets, and in which the rate of planetesimal accretion is calculated rather than prescribed. To do the latter, we must, of necessity, choose a particular model of planetesimal accretion. We selected the accretion model of Lissauer (1987) for the following reasons. First, it offers a promising means of solving the time scale problems alluded to above. Second, it represents a contrasting extreme from the prior assumption of a constant planetesimal accretion rate and so offers an opportunity to examine whether there is a qualitative difference in the results and, it is hoped, to bracket reality. The calculations carry the evolution beyond the crossover mass into the phase of rapid gas accretion; they do not include the final phase where gas accretion terminates; thus, they do not attempt to explain the final masses of Jupiter and Saturn. Preliminary reports of the results presented in this paper were given by Podolak *et al.* (1993) and Lissauer *et al.* (1995).

2. PROCEDURE

To simulate the concurrent gas and solid accretion of the giant planets, we used an evolutionary model having three major components: a calculation of the three-body accretion rate of a single dominant-mass protoplanet surrounded by a large number of planetesimals; a calculation of the interaction of accreted planetesimals with the gaseous envelope of the growing giant protoplanet; and a calculation of the gas accretion rate using a sequence of quasi-hydrostatic models having a core/envelope structure. These three components of the calculation were updated every time step in a self-consistent fashion in which relevant information from one component was used in the other components. We now describe these components, the key input quantities, and the limitations of our simulations.

2.1. Planetesimal Accretion

The early growth of the terrestrial planets from a swarm of planetesimals is thought to have involved "runaway" growth, in which there was a single dominant mass that grew rapidly from the accretion of nearby planetesimals (Greenberg *et al.* 1978, 1984). The time scale associated with this phase of the formation of the planets was short

because the relative velocity of the planetesimals, v_{rel}, was small compared with the escape velocity from the surface of the embryonic planet, v_{esc}, and hence the planet's gravitational cross section far exceeded its geometrical cross section. The runaway ended when the embryonic planet substantially depleted its ''feeding zone.'' The final phase of accretion of the terrestrial planets involved interacting embryos, with much higher values of v_{rel} and hence much longer time scales. Lissauer (1987) suggested that the giant planets may have had sufficient material in their nearby feeding zones so that they were able to reach M_{cross} during the runaway planetesimal accretion phase. Our specific assumptions are (1) there is a single accreting planet with $v_{rel} < v_{esc}$ and (2) the surface density of the planetesimal disk is a few times as large as that of the ''minimum mass'' solar nebula. As a result of these assumptions, there is a runaway phase during which M_{cross} is not quite reached.

According to the classical theory of Safronov (1969), a solid protoplanet grows by accreting planetesimals whose orbits cross its orbit at a rate given by

$$\frac{dM_p}{dt} = \pi R_c^2 \sigma \Omega F_g. \tag{1}$$

In Eq. (1), M_p is the mass of the giant protoplanet, R_c is its effective or capture radius, σ is the surface mass density of planetesimals, Ω is the orbital frequency, and F_g is the ratio of the gravitational cross section to the geometric cross section (''gravitational enhancement factor''). According to Kepler's laws of motion,

$$\Omega \propto a^{-3/2}, \tag{2}$$

where a is the semimajor axis of the protoplanet. In many models, the time scales for planet growth increase steeply with increasing distance from the Sun because of the dependence of Ω on a and because σ is expected to decrease with increasing a (Safronov 1969, Weidenschilling 1977). Time scale estimates for the Uranus/Neptune region exceed 10^9 years (Safronov 1969). However, time scales for giant planet formation that are consistent with the lifetime of the solar nebula may be achieved if σ is somewhat enhanced above its value for a so-called ''minimum''-mass solar nebula and if core growth takes place preferentially during the runaway planetesimal accretion phase when F_g can be very large (up to 10^4) (Lissauer 1987, 1993).

We considered a forming giant planet surrounded by planetesimals, all having equal masses and radii, m_p and r_p, situated in a disk of spatially constant (but time varying) mass density σ. It was assumed that $m_p \ll M_p$. Accurate values of F_g for this situation have been obtained by Greenzweig and Lissauer (1992). They did so by performing a large number of three-body (Sun, protoplanet, and planetesimal) orbital integrations where the planetesimals had a Rayleigh distribution of eccentricities and inclinations. In our simulations, we used analytical expressions for F_g that they derived as fits to their numerical calculations (cf. Greenzweig 1991): F_g is a function of i_H, e_H, and d_c, where i_H is the rms value of the planetesimals' orbital inclinations, e_H is the rms value of the planetesimals' orbital eccentricities, and d_c is the planetary embryo's effective capture radius for planetesimals. All three parameters are expressed in Hill sphere units

$$i_H \equiv \frac{a}{R_H} i, \tag{3a}$$

$$e_H \equiv \frac{a}{R_H} e, \tag{3b}$$

$$d_c \equiv \frac{R_c}{R_H}, \tag{3c}$$

where R_H, the Hill sphere radius, is given by

$$R_H = a \left(\frac{M_p}{3M_\odot} \right)^{1/3}, \tag{4}$$

where $M_\odot$ is the mass of the Sun.

According to the calculations of Greenzweig and Lissauer (1990, 1992), the planetesimals' inclinations are controlled by their mutual gravitational scatterings, and their eccentricities are determined by a combination of these scatterings and gravitational interactions with the protoplanet at distances comparable to its Hill sphere radius. (Note that because of the coherence of the orbital motions of the planetesimals and protoplanet, gravitational interactions well within the protoplanet's Hill sphere are not effective in pumping up the planetesimals' eccentricities to large values.) In particular, we use the prescription

$$i_H = \frac{v_{escp}}{\sqrt{3}\Omega R_H} \tag{5}$$

$$e_H = \max(2i_H, 2) \tag{6}$$

where v_{escp} is the escape velocity from the surface of a planetesimal.

The planet's accretion (feeding) zone was assumed to be an annulus that extended a radial distance, a_f, on either side of its orbit. According to the simulations of Greenzweig and Lissauer (1990; cf. Kary and Lissauer 1994), a_f is well approximated by

$$a_f = \sqrt{12 + e_H^2}\, R_H. \tag{7}$$

Thus, the accretion zone grows as the planet gains mass (independent of whether the accreted mass is solid or gas). The mass of planetesimals in the accretion zone is assumed

to equal the initial mass of planetesimals in the (current) accretion zone minus the amount that has already been accreted by the protoplanet; radial migration of planetesimals into and out of the accretion zone is therefore neglected. Random scatterings are assumed to spread the unaccreted planetesimals within the protoplanet's reach uniformly over its accretion zone, so that the formulas for F_g given in Appendix B of Greenzweig and Lissauer (1992) are applicable.

2.2. Interaction of Planetesimals with the Protoplanet

The presence of a gaseous envelope around the high-Z core of a forming giant planet can enhance the capture radius R_c, and can lead to the deposition of mass and energy within the envelope when its mass is large enough. More precisely, these effects begin to occur when an incoming planetesimal intercepts a mass of gas comparable to its own mass (Pollack *et al.* 1986). We used the orbit trajectory code of Podolak *et al.* (1988) to evaluate these types of interactions of planetesimals with the protoplanet's envelope. Here we summarize the protocols used.

According to the calculations of Safronov (1969), the initial relative velocity of a planetesimal far from the protoplanet, on average, is given by

$$v_i = \sqrt{\frac{5e^2}{8} + i^2}\, v_k, \tag{8}$$

where v_k is the protoplanet's Keplerian velocity about the Sun. This velocity was divided by $\sqrt{2}$ to approximately account for the greater accretion rates of those planetesimals in the velocity distribution that have lower e and i. For various trial values of the impact parameter, the trajectory program used the analytical solution of the two-body problem (planetesimal, planet) for no gas drag to determine the planetesimal's velocity vector at the point at which it reached the outer boundary of the protoplanet, R_p, which is evaluated in the protoplanet structure code (cf. Subsection 2.3). Once the planetesimal entered the protoplanet's envelope, its trajectory was found by a numerical integration of the equations of motion with allowance for the gravitational field of the core and envelope and for gas drag. We used the dependence of the gas drag force on Mach and Reynolds numbers that is given in Podolak *et al.* (1988). The equations of motion were integrated with a fourth-order Runge–Kutta scheme, whose time step equalled a fraction of the local Keplerian period. This choice of time step ensured that smaller time steps were used close to the core, where more temporal resolution was desirable.

Critical values for the impact parameter and the associated value of R_c (= periapsis altitude) were obtained in an iterative fashion by finding the largest value of the impact parameter for which the planetesimal was captured. The criterion for capture was that at the end of the planetesimal's first pass through the protoplanet's envelope, its total energy (kinetic plus gravitational) was less than a small negative number. This number, E_{esc}, was set by the condition that the planetesimal had enough energy at R_H to escape into a solar orbit:

$$E_{esc} = -3m_p\Omega^2 R_H^2. \tag{9}$$

Strictly speaking, this equation applies to escape along the Sun–protoplanet line. However, the minimum energy needed for escape is close to zero in all directions.

Having established the value of the critical impact parameter, we next carried out a set of trajectory calculations for a series of impact parameters that lay between zero and the critical value. For each choice of impact parameter, we followed the trajectory of the planetesimal until it either reached the surface of the core or totally vaporized in the protoplanet's envelope. Over the course of the trajectory, we kept track of the amount of mass vaporized within each mass shell of the envelope and the amount of energy deposited into each mass shell. We then averaged these results over the ensemble of impact parameters to determine a mean value for mass and energy deposition in each shell of the protoplanet and at the core interface.

In detail, our protocol for evaluating the mass and energy deposition profile of a planetesimal along its trajectory through the protoplanet's envelope was as follows. In accord with the properties of comet Halley, we pictured the planetesimal as consisting of small bits of rock and organic matter embedded in a matrix of water ice (e.g., Jessberger *et al.* 1989). In this case, the ice acted as the "glue" that held the planetesimal together. The surface temperature of the planetesimal was computed under the assumption of balance between heating and cooling, where heating includes gas drag and thermal radiation from the environment and cooling includes radiation emitted from the planetesimal surface and latent heat required to vaporize water ice. The emissivity of the small grains was assumed to be unity. Vaporization occurred at a rate set by the surface temperature and the associated vapor pressure (Podolak *et al.* 1988). When a layer of ice was vaporized, any rock or organics contained in that layer were also released into the envelope (referred to as "ablated material"). Their fate then depended on the local ambient temperature, T_{env}. When T_{env} exceeded the vaporization temperature of the ice, rock, or organics, (T_{ice}, T_{rock}, and T_{CHON}, respectively), these materials vaporized, extracting energy from the layer in the case of rock and ice, and releasing energy in the case of organics (as a result of chemical reactions with the ambient gas). Otherwise solid material kept sinking slowly into the deeper regions of the envelope, releasing gravitational energy (through drag heating). Energy was also

added to each mass shell corresponding to the conversion of kinetic energy into heat by the gas drag on the remaining planetesimal. Finally, the planetesimal was assumed to be fragmented into small (digestable) pieces when the gas dynamical pressure exceeded the compressional strength of the planetesimal.

Based on the above discussion, the amount of energy released into a given mass shell i by the passage of a planetesimal and its associated debris, ΔE_i, is given by

$$\Delta E_{\rm i} = F_{\rm d}\, ds_i + \sum_{j=1}^{3} X_j\, \Delta m_i (0.5 v_{\rm p}^2 - L_j \delta_{ij}) + \sum_{j=1}^{3} \sum_{i'=1}^{i} X_j\, \Delta m_{i'} \left(\delta'_{i'j} GM_i \left(\frac{1}{R_i} - \frac{1}{R_{i-1}} \right) - L_j \delta''_{i'j} \right), \tag{10}$$

where $F_{\rm d}$ is the drag force exerted on the planetesimal in layer i, ds_i is the path length through layer i, X_j is the mass fraction of planetesimal constituent j, Δm_i is the total mass of the planetesimal vaporized and ablated in shell i, $v_{\rm p}$ is the local velocity of the planetesimal, L_j is the latent heat of phase change of constituent j, δ_{ij} is a Kronecker delta that equals 1 when constituent j undergoes a phase change in layer i and is 0 otherwise, $\Delta m_{i'}$ is the total mass of the planetesimal ablated in shell i', $\delta'_{i'j}$ is the Kronecker delta that equals 1 when constituent j is ablated in layer i' and reaches layer i, G is the gravitational constant, M_i is the mass interior to mass shell i (envelope plus core), R_i is the distance of mass shell i from the protoplanet's center, and $\delta''_{i'j}$ is the Kronecker delta that equals 1 when constituent j ablates in mass shell i' and vaporizes in mass shell i. The first term on the right-hand side of Eq. (10) represents heating of a mass shell by gas drag slowing of the planetesimal, the second term represents heating due to the dissipation of the kinetic energy of the ablated material and cooling due to phase changes, and the third term represents heating due to gravitational energy release by sinking material that has ablated in layers above layer i and cooling by phase changes of this material.

In applying the above equation for the energy added to each mass shell of the envelope, we considered two limiting cases concerning the ultimate fate of the ablated material. In fact the result will depend on whether the shell is radiative or convective and on the relative time scales of settling and mixing. On the one hand, once a given constituent of the ablated material is vaporized, it may be rapidly mixed with the surrounding H- and He-rich gas, in which case it will remain within the mass shell where it vaporized. Alternatively, mixing with environmental gas may be sufficiently sluggish that vaporized material continues to sink because its molecular weight is greater than that of the envelope. In this case, we allow vaporized material to sink all the way to the core interface, releasing gravitational energy as it does so. For brevity, we refer to these cases as the "no sinking" and "sinking" cases. In either case, we add the mass of the planetesimal to the core, since our protoplanet structure code is not yet equipped to handle compositionally varying equations of state and opacity. Thus, in this one respect, the no sinking case is not strictly self-consistent. The effect of the dissolved material on the overall structure could be significant up to the time of crossover, and it will be considered in future calculations.

Any remnant planetesimal that intersects the core releases its kinetic energy as heat at the core's interface and uses up energy in phase changes that involve latent heat. We smear the net heating from this source and sink over a distance of one core radius into the envelope for reasons of numerical stability, as was done in our earlier calculation (BP86).

Table I summarizes the physical and chemical properties of the planetesimals used in our calculations. They are based on the most common types of materials found in comets, with special emphasis on the *in situ* measurements of comet Halley by the Giotto and Vega spacecraft (Jessberger *et al.* 1989, Pollack *et al.* 1994). It is fortunate that the results of this paper do not depend sensitively on the precise properties given in this table, given that the composition of the average comet is not known and may not represent a precise analog of the high-Z material from which the planets formed.

2.3. Gas Accretion

We constructed a time series of quasi-equilibrium core/envelope models of forming giant planets to determine the rate at which gas was accreted from the surrounding solar nebula. The mass and radius of the core were set by the cumulative mass of planetesimals that had been accreted up until the time of current interest and by the assumed density of the core, $\rho_{\rm core}$. A value of 3.2 g/cm^3 was used for $\rho_{\rm core}$, in accord with the materials composing the planetesimals and the high pressures and temperatures at the core interface (BP86). Our results do not depend sensitively on this choice.

We used the same set of equations of state and opacity coefficients for the envelope gases as were used in BP86. The equations of state allow for dissociation, ionization (including H metalization), and nonideal gas effects and are based on detailed thermodynamical calculations (Graboske *et al.* 1975, Grossman *et al.* 1980). These equations of state apply to a solar mixture of elements, $X = 0.74$, $Y = 0.243$, $Z = 0.017$. Our opacity sources included small grains made of water ice, silicates, and iron for temperatures up to 1700 K, molecules (H_2O, TiO) for temperatures up to 3000 K, and normal stellar sources at still higher temperatures (Alexander 1975, Alexander *et al.* 1983, Cox and Stewart 1970). These opacities are based on a solar mixture of elements; in particular, a solar abundance of

grains with approximately an interstellar size distribution is assumed. They do not include effects of organic grains or pressure-induced transitions of molecular hydrogen. Updated opacities for the range 800–10,000 K (Alexander and Ferguson 1994) were not yet available at the time these calculations were made, but these improved opacity estimates will be included in future calculations.

Since we might expect that most of the small grains initially present in the outer part of the solar nebula would have already accreted into larger objects at the time of the start of our calculations, it may appear to be inconsistent for us to use the opacity of a solar mixture of small (less than a few tens of microns) grains. However, we point out that a significant fraction of the mass of the grains in the coma of comets have sizes in the "small" size regime (Mazets *et al.* 1987, McDonnell *et al.* 1987). Thus, large amounts of small grains should have been released by planetesimal ablation in the outer envelopes. Furthermore, collisions of planetesimals produced ejecta containing small particles in the surrounding solar nebula. Clearly, however, it is difficult to estimate the amount of small grains present in the outer envelopes of the forming giant planets (see Lissauer *et al.* 1995 for a more detailed discussion of this important topic). Fortunately, the simulations of giant planet formation by BP86 suggest that key results, such as the value of the $M_{\rm cross}$, do not depend sensitively on the amount of grain opacity. In particular, reducing the grain opacity by a factor of 50 led to only a 25% reduction in $M_{\rm cross}$; a further test reported below confirms the insensitivity of $M_{\rm cross}$ but shows that the evolutionary time scale can be strongly affected. Finally, we note that grain opacity exceeds that due to H_2 as long as the abundance of small grains is more than 10^{-4} that for a solar mixture and that including the opacity of organic grains would boost the grain opacity at low and intermediate temperatures ($<$650 K) by about a factor of 2 (Pollack *et al.* 1994).

Quasi-equilibrium models of the envelope were constructed by using the conventional stellar structure equations of mass and energy conservation, hydrostatic equilibrium, and the diffusion equation for radiative transfer (BP86). In convection zones the temperature gradient was approximated by the adiabatic gradient. The energy equation includes three sources: the heat generated by captured planetesimals, PdV work from compression by gravitational forces, and cooling from release of internal heat. The boundary conditions at the inner edge of the envelope are that the luminosity is zero, the mass equals the core mass, and the radius equals the core radius. The outer radius of the envelope, $R_{\rm p}$, is set equal to the smaller of the Hill sphere (tidal) radius, $R_{\rm H}$, defined in Eq. (4), and the accretion radius, $R_{\rm a}$, given by

$$R_{\rm a} = \frac{GM_{\rm p}}{c^2}, \tag{11}$$

where c is the sound speed in the solar nebula. As discussed in BP86, a gas parcel located outside of $R_{\rm a}$ has more thermal energy than gravitational energy binding it to the protoplanet. Hence, it is not part of the planet beyond $R_{\rm a}$ (or more precisely, it is no longer appropriate to use the equation of hydrostatic equilibrium). At $R_{\rm p}$, we require the envelope's density and temperature to equal those in the surrounding solar nebula, $\rho_{\rm neb}$ and $T_{\rm neb}$. In actuality, this condition will not be met precisely at either $R_{\rm a}$ or $R_{\rm H}$, but rather will reflect the complicated flow of the solar nebula near a protoplanet. Fortunately, our results depend very insensitively on these outer boundary conditions (Mizuno 1980, BP86).

Gas accretion occurs as a result of the contraction of the outer envelope and the steady increase in $R_{\rm p}$ as the planet's total mass increases. Gas from the surrounding solar nebula is assumed to flow freely into the evacuated volume at whatever rate is needed to restore the outer boundary conditions. Suppose that at time t the envelope has a radius $R_{\rm p}(t)$ that is consistent with the outer boundary conditions. During time step Δt, a planetesimal mass $\Delta m_{\rm p}$ is added to the planet, increasing the outer radius to R_{bd} (where $R_{bd} = \min[R_{\rm a}, R_{\rm H}]$), while the planet's radius contracts to $R_{\rm p}(t + \Delta t)$. Thus, an amount of gas, $\Delta m_{\rm neb}$, will be added that is given by

$$\Delta m_{\rm neb} = 4\pi R_{bd}^2 \rho_{\rm neb}[R_{bd} - R_{\rm p}(t + \Delta t)]. \tag{12}$$

The mass of the added gas causes R_{bd} to increase, and the gas is redistributed over the evacuated space in accord with the equation of hydrostatic equilibrium. Thus, we iteratively adjust the outer boundary and amount of added mass to obtain a self-consistent structure at time $t + \Delta t$.

2.4. Putting the Pieces Together

We have now described the protocols used for the three main parts of the calculation. Here, we indicate how these pieces interact and summarize the key parameters used in our simulations. We begin the calculation at $t = 0$, with an initial model of the planet those total mass (almost entirely high-Z) is comparable to that of Mars. Using the procedures outlined in BP86, we find a quasi-equilibrium structure for the envelope of this initial model that matches the specified time-invariant values of $\rho_{\rm neb}$ and $T_{\rm neb}$ at its outer boundary. We also specify the initial column mass density of planetesimals, $\sigma_{\rm init}$, their composition, and their radius, $r_{\rm p}$; planetesimal radii and composition are assumed to remain constant over the course of accretion (an obvious oversimplication). At $t = 0$, the surface density of the disk is assumed to be constant and, thus, we do not take into account the small decrease in the planetesimal surface density in the embryo feeding zone, which has already occurred as a result of the mass incorporated in the embryo. Tables

TABLE I
Properties of Planetesimals

	Component[a]			
Property	H_2O Ice	Rock	CHON	Total
mass fraction	0.397	0.308	0.295	1
density (g/cm^3)	0.92	3.45	1.5	1.39
latent heat[b] (erg/g)	[c]2.8×10^{10}	[c]8.08×10^{10}	[d] -7.0×10^{10}	1.54×10^{10}
vaporization temperature (K)	165	1500	650	-

[a] The three major components of the planetesimals are water ice, ferromagnesium silicates ("rock"), and organics ("CHON").
[b] The latent heats of ice and rock are endothermic, whereas that of the CHON is exothermic.
[c] Podolak *et al.* (1988).
[d] Estimated.

I and II summarize the key parameters that are used in the calculation and their nominal set of values.

We next wish to find a new equilibrium model at the end of time step Δt, determining the rates of planetesimal and gas accretion in the process. To do this, we first use the formulas for three-body accretion to determine the mass of accreted planetesimals. In so doing, we use the properties of the model of the planet at the beginning of the time step to determine R_c and e_H. Then, we use the trajectory code to evaluate the mass and energy deposited by the accreting planetesimals in each shell of the protoplanet's envelope and at the core interface. In doing this calculation, we use a preliminary updated envelope structure that takes account of the added planetesimal and gas masses (and an associated rezoning of the mass shells). For a particular sequence, we choose either the sinking or no-sinking option for the vaporized material from the planetesimals in the envelope. Finally, the energy profile found from the trajectory calculations is used to calculate a final equilibrium structure for the envelope.

TABLE II
Key Model Parameters and Their Nominal Values

Parameter	Nominal Value
orbital distance	5.2 A. U.
planetesimal radius	100 km
other planetesimal properties	see Table I
initial planetesimal surface density	10 g/cm^2
fate of dissolved planetesimal	sinks to core interface
nebula temperature	150 K
nebula density	5.0×10^{-11} g/cm^3

We now have a new model for the protoplanet and are ready to take the next time step. First, we readjust the column mass density of planetesimals to allow for the mass that has been accreted in the previous time step and the

TABLE III
Input Parameters

case	$\sigma_{init,Z}$ (g/cm^2)	$\sigma_{init,XY}$ (g/cm^2)	r_p (km)	a (A.U.)	T_{neb} (K)	ρ_{neb} (g/cm^3)	δ_s
J1	10.	700.	100	5.203	150	5.0×10^{-11}	1
J1a[a]	10.	700.	100	5.203	150	5.0×10^{-11}	1
J1b[b]	10.	700.	100	5.203	150	5.0×10^{-11}	1
J1c[c]	10.	700.	100	5.203	150	5.0×10^{-11}	1
J2	7.5	525.	100	5.203	150	5.0×10^{-11}	1
J3	15.	1050.	100	5.203	150	5.0×10^{-11}	1
J4	10.	700.	100	5.203	150	5.0×10^{-11}	0
J5[d]	10.	700.	100	5.203	150	5.0×10^{-11}	1
J6[e]	10.	700.	100	5.203	150	5.0×10^{-11}	1
J7	10.	700.	1	5.203	150	5.0×10^{-11}	1
J8	10.	700.	1	5.203	150	5.0×10^{-11}	0
S1	3.	210.	100	9.539	100	2.5×10^{-11}	1
S2	3.	210.	100	9.539	100	2.5×10^{-11}	0
U1	0.75	52.5	100	19.18	75	1.0×10^{-11}	1
U2	0.75	52.5	1	19.18	75	1.0×10^{-11}	1

[a] Planetesimal accretion arbitrarily stopped at 1.5 myr.
[b] Planetesimal accretion arbitrarily stopped at 3.5 myr.
[c] Planetesimal accretion arbitrarily stopped at 6.8 myr.
[d] All planetesimals reach the core and energy is deposited within one core radius of core–envelope boundary.
[e] Grain opacity in the envelope equals 2% of nominal (solar composition) value.

TABLE IV
Results

	FIRST MAXIMUM			END OF PHASE 1				CROSS-OVER POINT				ENDPOINT				
run	Time[a]	M_{XY}[b]	M_Z	Time	M_{XY}	M_Z	$\dot{M}_{XY}=\dot{M}_Z$[c]	Time	M_{cross}	$\dot{M}_{XY}$	$\dot{M}_Z$	Time	M_{XY}	M_Z	$\dot{M}_{XY}$	$\dot{M}_Z$
J1	0.485	3.3×10^{-3}	6.96	0.61	0.16	11.4	5.1×10^{-6}	7.58	16.17	1.2×10^{-5}	2.7×10^{-6}	8.00	64.4	21.5	7.3×10^{-3}	3.7×10^{-4}
J1a	〃	〃	〃	〃	〃	〃	〃	3.32	12.24	3.0×10^{-5}	0.	3.54	29.8	12.2	3.3×10^{-4}	0.
J1b	〃	〃	〃	〃	〃	〃	〃	4.60	13.04	6.1×10^{-5}	0.	4.76	34.3	13.0	1.0×10^{-3}	0.
J1c	〃	〃	〃	〃	〃	〃	〃	7.07	14.94	9.7×10^{-5}	0.	7.16	34.3	14.9	2.7×10^{-3}	0.
J2	0.580	8.4×10^{-4}	4.65	0.81	0.08	7.4	1.0×10^{-6}	48.0	10.51	1.3×10^{-6}	2.3×10^{-7}	50.0	15.8	11.4	1.1×10^{-6}	6.9×10^{-6}
J3	0.388	1.6×10^{-2}	12.1	0.45	0.65	21.0	2.5×10^{-5}	1.51	29.61	1.2×10^{-4}	3.1×10^{-5}	1.57	56.0	33.8	1.1×10^{-3}	1.5×10^{-4}
J4	0.485	9.1×10^{-3}	7.2	0.59	0.36	11.5	6.9×10^{-6}	1.86	16.07	6.3×10^{-5}	1.8×10^{-5}	1.93	48.2	19.7	5.1×10^{-3}	3.7×10^{-4}
J5	0.489	4.0×10^{-3}	7.18	0.63	0.23	11.5	3.4×10^{-6}	7.65	16.17	1.2×10^{-5}	2.9×10^{-6}	8.00	38.2	19.3	1.5×10^{-3}	9.0×10^{-5}
J6	0.465	1.1×10^{-2}	7.56	0.55	0.30	11.5	8.7×10^{-6}	2.75	16.18	1.8×10^{-5}	3.9×10^{-6}	2.88	19.4	16.8	2.6×10^{-5}	5.2×10^{-6}
J7	0.214	7.9×10^{-4}	5.64	0.26	0.14	11.5	7.1×10^{-6}	6.94	16.18	5.0×10^{-6}	2.8×10^{-6}	7.31	44.7	20.22	1.1×10^{-3}	1.1×10^{-4}
J8	0.214	3.0×10^{-3}	5.44	0.26	0.62	11.6	1.4×10^{-5}	1.22	16.07	2.6×10^{-4}	3.3×10^{-5}	1.25	34.2	18.6	2.5×10^{-3}	2.4×10^{-4}
S1	1.90	7.9×10^{-3}	7.49	2.48	0.45	11.7	1.5×10^{-6}	9.50	16.34	1.0×10^{-5}	2.7×10^{-6}	9.80	23.2	17.5	4.2×10^{-5}	7.0×10^{-6}
S2	1.87	4.6×10^{-2}	7.31	2.23	1.11	11.7	5.0×10^{-6}	3.24	15.87	1.1×10^{-4}	1.7×10^{-5}	3.29	27.0	17.33	6.8×10^{-4}	5.3×10^{-5}
U1	12.9	3.4×10^{-2}	7.32	15.2	0.83	11.7	8.7×10^{-7}	21.9	16.24	2.8×10^{-5}	2.6×10^{-6}	22.05	21.9	16.86	8.3×10^{-5}	6.3×10^{-6}
U2	0.476	2.3×10^{-3}	5.48	0.92	0.48	11.9	1.8×10^{-6}	6.69	16.57	1.2×10^{-5}	3.3×10^{-6}	6.94	26.9	18.07	1.7×10^{-4}	1.6×10^{-5}

[a] Time is in units of millions of years, myr.
[b] Mass is in units of Earth's mass, $M_\oplus$.
[c] Accretion rate is in units of Earth masses per year, $M_\oplus$/year.

expansion of the feeding zone (see Section 2.1). Then, we follow the same sequence of steps to obtain a new model of the protoplanet and the new rates of planetesimal and gas accretion.

2.5. *Key Assumptions*

Here, we summarize key assumptions made in our simulations and define their basic limitations. These include:

1. The opacity in the outer envelope is determined by a solar mixture of small grains. We will comment below on the effects of a change in the abundance of small grains. We also assume solar abundances in calculating the opacity in deeper regions of the envelope where molecular opacities dominate. Here, we may have underestimated the true opacity throughout much of the accretion (e.g., enhanced amounts of dissolved H_2O would raise the opacity).

2. The equation of state for the envelope is that for a solar mixture of elements. This will start to become a questionable assumption when a large amount of planetesimal mass has dissolved in the envelope. For example, the composition gradient introduced by the distribution of dissolved heavy material could affect the extent of convection zones. But, variations in the equation of state resulting from the addition of dissolved high-Z material probably affected the evolution of the planet far less than the changes in the opacity due to the same addition of high-Z material.

3. During the entire period of growth of a giant planet, it is assumed to be the sole dominant mass in the region of its feeding zone, i.e., there are no competing embryos, and planetesimal sizes and random velocities remain small. A corollary of this assumption is that accretion can be described as a quasi-continuous process, as opposed to a discontinuous one involving the occasional accretion of a massive planetesimal.

4. Planetesimals are assumed to be well mixed within the planet's feeding zone, which grows as the planet's mass increases, but planetesimals are not allowed to migrate into or out of the planet's feeding zone as a consequence of their own motion. Tidal interaction (Lin and Papaloizou 1993) between the protoplanet and the disk, or migration of the protoplanet, is not considered. It is not at all obvious that these various assumptions are valid, but no well-defined quantitatively justifiable alternative assumptions are available.

5. Hydrodynamic effects are not considered in the evolution of the envelope. Although Wuchterl (1991) found that dynamical instability occurred in his models once the envelope mass became comparable to the core mass, most of the present results are based on the phases before the crossover mass is reached.

3. RESULTS

In this section, we first present the results for a baseline simulation in some detail and then examine the sensitivity of the results to variations in key parameters. Table III states the parameters for each case and Table IV gives basic results. In all cases, the simulations begin with a protoplanet having a mass comparable to that of Mars with almost all its mass in a high-Z core. We continue the evolution past the onset of runaway gas accretion, which operationally is defined by the point where the gas accretion rate exceeds the planetesimal accretion rate by a factor of 10 and is increasing in a quasi-exponential fashion with time.

We judge the applicability of a given simulation to planets in our Solar System using two basic yardsticks. One yardstick is provided by the time required to reach the runaway gas accretion phase. This time interval should be less than the lifetime of the gas component of the solar nebula, t_{sn}, for successful models of Jupiter and Saturn and greater than t_{sn} for successful models of Uranus and Neptune. Limited observations of accretion disks around young stars suggest that $t_{sn} \lesssim 10^7$ years, based on observations of the dust component. The lifetime of the gas component is less well constrained observationally (Strom *et al.* 1993).

A second yardstick is provided by the amount of high-Z mass accreted, M_Z. In the case of Jupiter and Saturn, M_Z at the end of a successful simulation should be comparable to, but somewhat smaller than, the current high-Z masses of these planets, since additional accretion of planetesimals occurred between the time they started runaway gas accretion and the time they contracted to their current dimensions and were able to gravitationally scatter planetesimals out of the Solar System. Thus, reasonable values of M_Z for Jupiter and Saturn are $\sim$10–30$M_\oplus$ and 10–20$M_\oplus$, respectively. In the cases of Uranus and Neptune, reasonable values for M_Z would be somewhat less than their current high-Z masses at a time when the low-Z mass M_{XY} falls in the range 1–2$M_\oplus$. A reasonable value of M_Z for these two planets is $\sim 10 M_\oplus$.

3.1. Baseline Model for Jupiter

Our baseline model (case J1), which uses the parameters given in Tables I and II, is meant to provide a reasonable simulation of the formation of Jupiter, as judged by the yardsticks defined above. Figure 1a shows the evolutionary behavior of the masses M_{XY} and M_Z. (Note that values quoted for M_{XY} refer to all of the mass accreted in the gas phase and, thus, they include a small fraction of heavy elements.) Figure 1b shows the planetesimal accretion rate (dM_Z/dt) and the gas accretion rate (dM_{XY}/dt) for this baseline model, and Fig. 1c illustrates the luminosity. According to these figures, there are three main phases to the accretion of our model Jupiter. Phase 1 is characterized by rapidly varying rates of planetesimal and gas accretion. Throughout phase 1, dM_Z/dt exceeds dM_{XY}/dt. Initially, there is a very large difference (many orders of magnitude) between these two rates; however, they become progressively more comparable as time advances. Over much of phase 1, dM_Z/dt increases steeply. After a maximum at 5×10^5 years, it declines sharply. Meanwhile, dM_{XY}/dt keeps steadily growing by many orders of magnitude from its extremely low initial value.

The second phase of accretion is characterized by relatively time-invariant values of dM_Z/dt and dM_{XY}/dt, with $dM_{XY}/dt > dM_Z/dt$. We note that the small fluctuations in the accretion rates that are particularly noticeable during this phase (Fig. 1b) are a numerical artifact that stems from the iterative scheme used to adjust R_p (the actual planetary radius) to have a value approximately equal to R_{bd}. Finally, phase 3 is defined by rapidly increasing rates of gas and planetesimal accretion, with dM_{XY}/dt exceeding dM_Z/dt by steadily increasing amounts.

Insights into the physics that controls the accretion rates during the three phases (but especially phase 1) may be obtained if one examines the evolutionary behavior of the surface density of planetesimals (Fig. 1d) within the protoplanet's feeding zone, σ_Z. Initially, before σ_Z decreases significantly, dM_Z/dt is expected to increase rapidly due to an increase in the capture radius of the growing protoplanet (e.g., Lissauer 1987, Wetherill and Stewart 1989). The planetesimal capture radius, R_c, initially simply equals R_{core} and

$$\frac{dM_Z}{dt} \propto R_{core}^4 \propto M_Z^{4/3} \tag{13}$$

when gravitational focusing is taken into account in the two-body approximation. But later, when the envelope becomes sufficiently massive, planetesimals are captured by gas drag and, hence, R_c exceeds R_{core} by progressively larger amounts (cf. Fig. 1e). As a result, dM_Z/dt increases even more rapidly with time.

A decline in dM_Z/dt begins when the cumulative amount of accreted high-Z material becomes a significant fraction of the mass initially contained within the *current* boundaries of the feeding zone. Such a depletion is inevitable within the context of our assumptions about the source of planetesimals, since the mass of material within the feeding zone is roughly proportional to R_H [Eq. (7)] and $R_H \propto M_p^{1/3}$ [Eq. (4)]. The sharp decline of σ_Z with time in Fig. 1d is the result of a progressive and ultimately nearly complete depletion of planetesimals in the protoplanet's feeding zone brought about by prior accretion. Thus, phase 1 of our evolutionary simulations denotes the period during which runaway planetesimal accretion occurs, and it ends

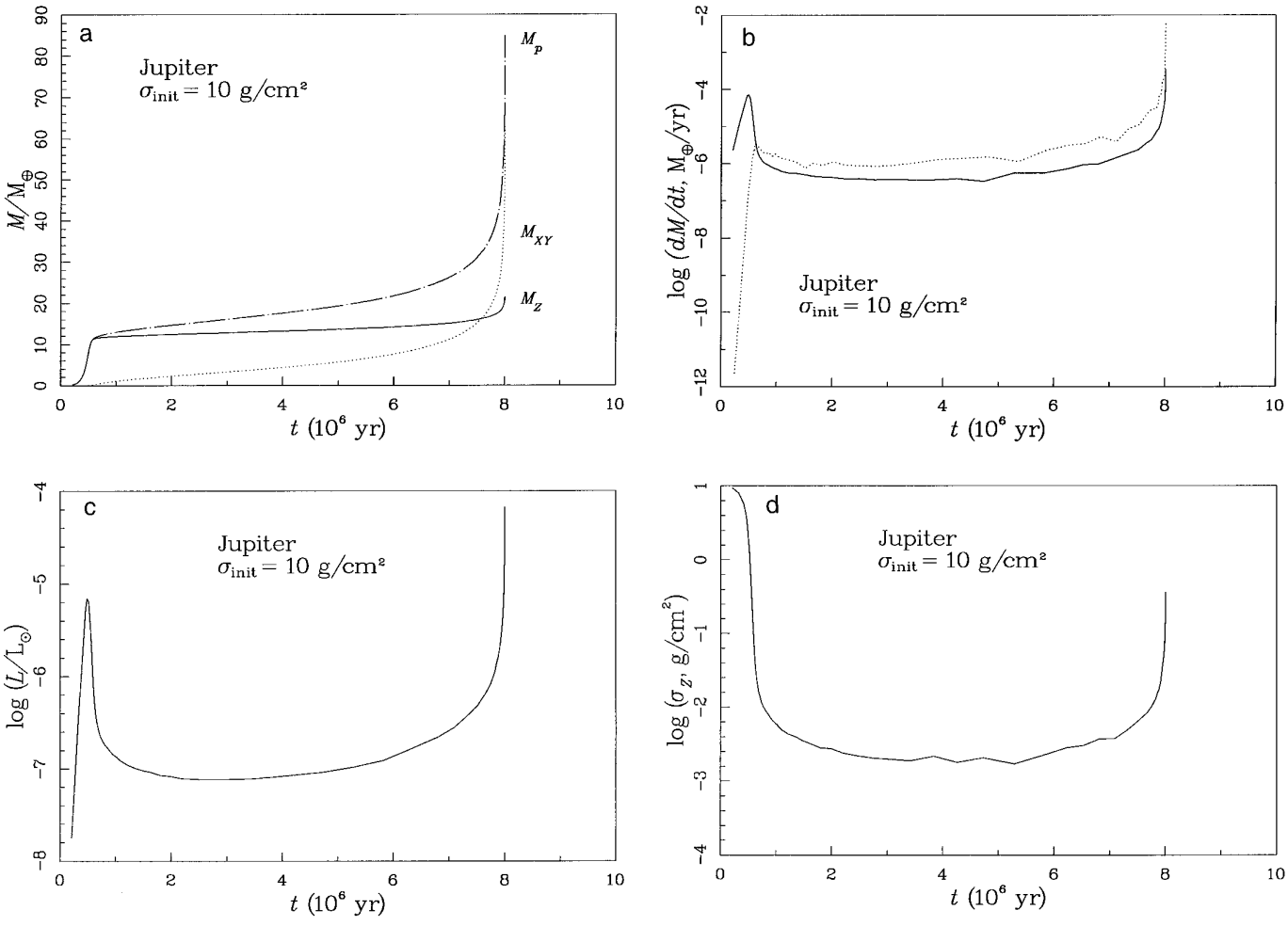

FIG. 1. (a) Planet's mass as a function of time for our baseline model, case J1. In this case, the planet is located at 5.2 AU, the initial surface density of the protoplanetary disk is 10 g/cm^2, and planetesimals that dissolve during their journey through the planet's envelope are allowed to sink to the planet's core; other parameters are listed in Table III. The solid line represents accumulated solid mass, the dotted line accumulated gas mass, and the dot–dashed line the planet's total mass. The planet's growth occurs in three fairly well-defined stages: During the first $\sim 5 \times 10^5$ years, the planet accumulates solids by rapid runaway accretion; this "phase 1" ends when the planet has severely depleted its feeding zone of planetesimals. The accretion rates of gas and solids are nearly constant with $\dot{M}_{XY} \approx 2$–$3\dot{M}_Z$ during most of the $\sim 7 \times 10^6$ years' duration of phase 2. The planet's growth accelerates toward the end of phase 2, and runaway accumulation of gas (and, to a lesser extent, solids) characterizes phase 3. The simulation is stopped when accretion becomes so rapid that our model breaks down. The endpoint is thus an artifact of our technique and should not be interpreted as an estimate of the planet's final mass. (b) Logarithm of the mass accretion rates of planetesimals (solid line) and gas (dotted line) for case J1. Note that the initial accretion rate of gas is extremely slow, but that its value increases rapidly during phase 1 and early phase 2. The small-scale structure which is particularly prominent during phase 2 is an artifact produced by our method of computation of the added gas mass from the solar nebula. (c) Luminosity of the protoplanet as a function of time for case J1. Note the strong correlation between luminosity and accretion rate (cf. b). (d) Surface density of planetesimals in the feeding zone as a function of time for case J1. Planetesimals become substantially depleted within the planet's accretion zone during the latter part of phase 1, and the local surface density of planetesimals remains small throughout phase 2. (e) Four measures of the radius of the growing planetary embryo in case J1. The solid curve shows the radius of the planet's core, R_{core}, assuming all accreted planetesimals settle down to this core. The dashed curve represents the effective capture radius for planetesimals 100 km in radius, R_c. The dotted line shows the outer boundary of the gaseous envelope at the "end" of a timestep, R_p. The long- and short-dashed curve represents the planet's accretion radius, R_a.

when the protoplanet has virtually emptied its feeding zone of planetesimals.

If this simulation had been done in a gas-free environment, as might be appropriate for the formation of the terrestrial planets, then the next phase would have to involve interacting embryos for accretion to reach the desired culmination point (Lissauer 1987, Lissauer and Stewart 1993). However, it is possible to carry our simulations of the formation of the giant planets to a reasonable endpoint without involving interacting embryos, because of the im-

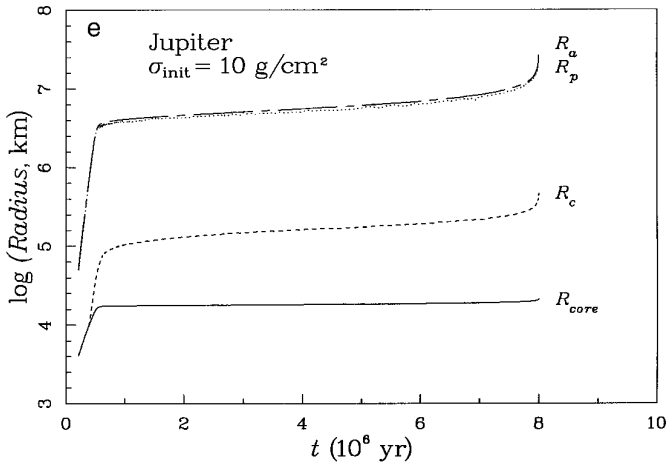

FIG. 1—*Continued*

pact of gas accretion on the subsequent evolution. In particular, the gaseous envelope is massive enough at the end of phase 1 for its contraction to lead to further gas accretion, which augments the planet's total mass. This results in a progressive increase of its Hill sphere radius, and hence, the size of its feeding zone keeps increasing, bringing new planetesimals within its sphere of influence. Thus, phase 2 involves a controlled interaction between the accretion rates of gas and planetesimals. The nature of phase 2 is of course dependent on assumption 3 of Section 2.5, namely, that there are no competing embryos in the neighborhood so that the supply of planetesimals is continuous. If this condition did not exist, then gas accretion during phase 2 would lead to merging of nearby embryos rather than smooth accretion of planetesimals. We will defer until Section 4.1 a discussion of the mechanisms that are responsible for the differences in accretion style during phases 2 and 3. Here, we simply note that phase 3 is analogous to the classical ''runaway'' gas accretion phase of earlier calculations (e.g., BP86). However, phase 2 is an entirely new phase that was not present in previous simulations of the formation of the giant planets. It represents the transition phase between runaway accretion of solids and runaway accretion of gas.

As can be seen from Figs. 1a and b, phase 1 lasts only about 6×10^5 years. This time scale, t_{ph1}, can readily be estimated from the set of equations (Lissauer 1987)

$$M_{iso} = C_1(a^2\sigma_{init})^{3/2}, \tag{14}$$

$$t_{ph1} = \frac{C_2 M_{iso}^{1/3}}{(\sigma_{init}\Omega F_g)}, \tag{15}$$

where M_{iso} is the planet's ''isolation mass'' (its mass after its feeding zone has been depleted), $C_1 = 1.56 \times 10^{25}$ g if σ_{init} is in units of g/cm^2 and a is in units of AU, and $C_2 = 8.126$ with all quantities in cgs units; σ_{init} is the initial surface density of planetesimals in the feeding zone; and other variables have been defined earlier. We obtained a large value of M_{iso} by selecting a σ_{init} that was somewhat larger than that given by a so-called minimum mass solar nebula and a small value for t_{ph1} by considering a situation where F_g is very large even at $t = 0$ due to the small random velocities of the planetesimals (Lissauer 1987).

At the end of phase 1, $M_Z \approx 12M_\oplus$ in agreement with Eq. (14), and $M_{XY} < 1M_\oplus$. Subsequently, in phase 2, M_Z increases by another $4M_\oplus$ and M_{XY} increases to a value essentially equal to that of M_Z. During phase 2, the surface density of the solids remains very small. The planetesimal accretion rate is thus essentially equal to the rate at which planetesimals enter the planet's accretion zone. The initial mass of planetesimals within the planet's accretion zone is proportional to the one-third power of the planet's mass, so during phase 2

$$M_Z + M_{XY} \propto M_Z^3. \tag{16}$$

Differentiating Eq. (16) with respect to time, we obtain the following relationship between the accretion rates of solids and gas during phase 2:

$$\dot{M}_Z \approx \left(2 + 3\frac{M_{XY}}{M_Z}\right)^{-1} \dot{M}_{XY}. \tag{17}$$

The numerical results (Fig. 1b) are consistent with this expression. It follows from Eq. (16) that the crossover mass, M_{cross}, at which $M_Z = M_{XY}$, is given by

$$M_{cross} \leq \sqrt{2}\, M_{iso}. \tag{18}$$

The inequality is present in Eq. (18) because some planetesimals reside within the planet's accretion zone when the crossover mass is reached. Note that the crossover masses

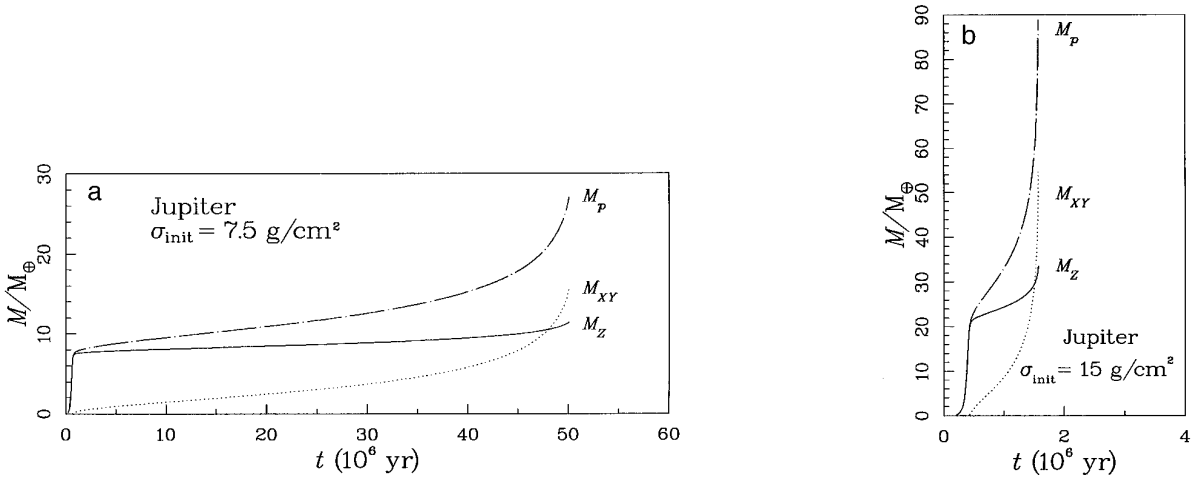

FIG. 2. (a) Cumulative mass of low-Z material (dots), high-Z material (solid), and total (dot-dash) as a function of time for case J2. The duration of phase 2 is a factor of 7 longer than in case J1 as a result of a 25% drop in initial surface mass density of planetesimals, and is inconsistent with the best available estimate of the lifetime of gas within the solar nebula, $t_{sn} \lesssim 10^7$ years. (b) Cumulative masses (as in a) as a function of time for case J3. The increase in the surface density of planetesimals by 50% relative to case J1 leads to a much more rapid progression through phase 2; however, the crossover mass, $M_{cross} \approx 30 M_\oplus$, may be larger than the amount of condensible material in Jupiter.

found in our simulations are always within a few percent of $\sqrt{2}$ times the mass at the end of phase 1 (cf. Table 4), except in those runs where we modified our procedure by terminating planetesimal accretion during phase 2.

Phase 2 lasts about 7×10^6 years. Thus, for our baseline model, the time required for the protoplanet to reach runaway gas accretion (phase 3) is determined almost solely by the duration of phase 2. This time scale is comparable to the estimated lifetime of the solar nebula, t_{sn}. In addition, the mass of high-Z material accumulated by the end of our simulation, $21.5 M_\oplus$, is comparable to or somewhat less than current estimates of M_Z for present-day Jupiter (Zharkov and Gudkova 1991, Chabrier *et al.* 1992). We conclude that our baseline model is consistent with the two basic yardsticks for judging the reasonableness of a simulation. Additional comparisons with observational and theoretical constraints will be made in Section 4.3.

3.2. Other Models for Jupiter

We now focus our attention on the effects of parameters that significantly influence the results of our simulations of the formation of the giant planets. These parameters include σ_{init}, δ_s, and a. The parameter δ_s equals 1 when we allow dissolved planetesimal-derived material to continue to sink toward the core and release gravitational energy; it equals 0 when this material is not allowed to sink. Effects of opacity, planetesimal size, and the outer boundary condition are also considered.

Figures 2a and b illustrate the great sensitivity of the accretion rates to variations in σ_{init} from its baseline value of 10 g/cm^2. Decreasing σ_{init} to 7.5 g/cm^2 (case J2) or increasing it to 15 g/cm^2 (case J3) greatly alters both the time it takes the protoplanet to reach the runaway gas accretion phase and the mass of high-Z material that it contains at this point. In particular, the interval of time from the start to the finish of our simulations, t_{end}, equals 5.0×10^7 years for the low-σ_{init} case (J2), 8.0×10^6 years for the nominal-surface-density case (J1), and 1.6×10^6 years for the high-σ_{init} case (J3). Thus, varying σ_{init} by only a factor of 2 results in a factor of 30 variation in t_{end}. Since t_{ph1} is relatively insensitive to σ_{init}, this effect is almost entirely determined by the duration of phase 2. The value of M_Z equals 11.4, 21.5, and $33.8 M_\oplus$ at $t = t_{end}$ for the low-, nominal-, and high-surface-density cases, respectively. Thus, varying σ_{init} by a factor of 2 produces a factor of 3 spread in M_Z, as expected from Eq. (14).

The great sensitivity of t_{end} and M_Z to σ_{init} makes it possible to place very tight constraints on the actual value of σ_{init} of the solar nebula, within the context of our basic assumptions. In particular, σ_{init} has to lie within a few tens of percent of 10 g/cm^2 at Jupiter's distance from the Sun for our simulations to be consistent with the two basic yardsticks for reasonableness of our results. If σ_{init} is $\lesssim$7.5 g/cm^2, then t_{end} exceeds t_{sn}. If $\sigma_{init} > 15$ g/cm^2, then the value of M_Z at t_{end} exceeds the current high-Z mass of Jupiter.

We next examine the sensitivity of our results to the value of δ_s (case J4). Figure 3 shows the evolutionary history of the masses when $\delta_s = 0$ (no sinking). Comparing these results with those shown in Fig. 1a for $\delta_s = 1$, we see that t_{end} is shortened by about a factor of 4 when the vaporized material is not allowed to sink. However, M_Z at

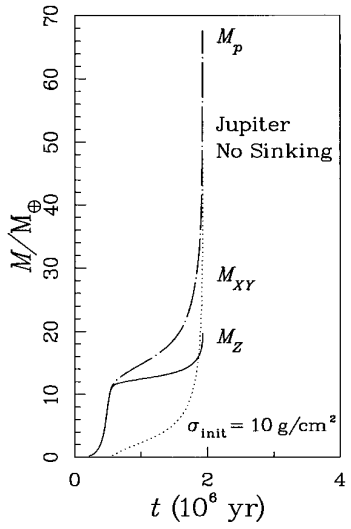

FIG. 3. Cumulative masses (as in Figs. 1a and 2) as a function of time for case J4. The duration of phase 2 is less than in case J1 because dissolved planetesimals do not sink, so less energy is available to support the planet's envelope against gravitational contraction.

$t = t_{end}$ for $\delta_s = 0$ ($19.7M_\oplus$) is essentially the same as its value for $\delta_s = 1$ ($21.5M_\oplus$), considering the fact that the latter case was evolved somewhat further. Thus, the bounds on acceptable values of σ_{init} for the no-sinking case remain the same on the high end and are slightly lower on the low end, in comparison with the corresponding bounds for the sinking case. In connection with the parameter δ_s, another test, case J5, was performed with the same parameters as in case J1 but under the assumption that all planetesimals reached the core and deposited their energy within one core radius of the core boundary; this procedure is that followed by BP86. The total energy released by planetesimal accretion is thus the same as in case J1, but the distribution in radius is somewhat different. The evolution is essentially the same as that for case J1.

In case J6, the grain opacity in the envelope is reduced by a factor of 50, although the molecular opacity, which dominates at temperatures above 1700 K, remains the same. The results for t_{ph1} and M_{cross} are hardly changed, but the time to transit phase 2 is only 2.2×10^6 years for case J6 as compared with 7.0×10^6 years for case J1. Thus, the overall evolutionary time scale is reduced by almost a factor of 3, indicating that the details of the opacity are in fact significant.

The effect of the outer boundary condition ρ_{neb} is tested by reducing it by a factor 10, leaving all other parameters the same as in case J1. As expected from previous numerical (BP86) and analytical (Stevenson 1982, Lissauer *et al.* 1995) results there is very little effect on the evolution. At $M_{XY} = M_Z$, the value of M_{cross} is practically identical to that in case J1, and the evolutionary time is a mere 1.7×10^5 years longer.

The effect of changing the assumed planetesimal size is considered in cases J7 and J8, which are calculated with $r_p = 1$ km and with $\delta_s = 1$ and 0, respectively. In both cases the isolation mass at the end of phase 1 is the same as in case J1, but the time is reduced by about a factor of 2, as a result of an enhanced gravitational focusing factor at early times. The time spent in phase 2 by case J7 is 6.7×10^6 years, practically the same as in case J1, while case J8 spent 1×10^6 years in this phase, slightly shorter than the corresponding time for the analogous case J4. Because most of the time is spent in phase 2, the effect of the planetesimal size on the evolution of Jupiter is small; however, it is much more important in the case of Uranus, which is discussed in the following subsection.

3.3. Models for Saturn and Uranus

We now assess the impact of distance from the Sun on our results by considering values of a that correspond to the current orbital semimajor axes of the giant planets. We first increase a from 5.2 to 9.5 AU, the value appropriate for Saturn (case S1). Since the current high-Z masses of Jupiter and Saturn are similar (Zharkov and Gudkova 1991, Chabrier *et al.* 1992), we want to pick a value for the isolation mass of Saturn that is comparable to the isolation mass of Jupiter for our nominal case. According to Eq. (14) for M_{iso}, we therefore need to scale σ_{init} approximately as a^{-2}.

Figure 4 shows the evolutionary history of the masses for our nominal Saturn model ($\sigma_{init} = 3$ g/cm^2). Not surprisingly, phase 1 for our nominal Saturn model lasts about four times longer than for our nominal Jupiter model; $\sigma_{init}\Omega$ is smaller by a factor of 8 but F_g is larger by a factor of 2 (cf. [Eq. (1)]. However, t_{end} is only slightly larger for

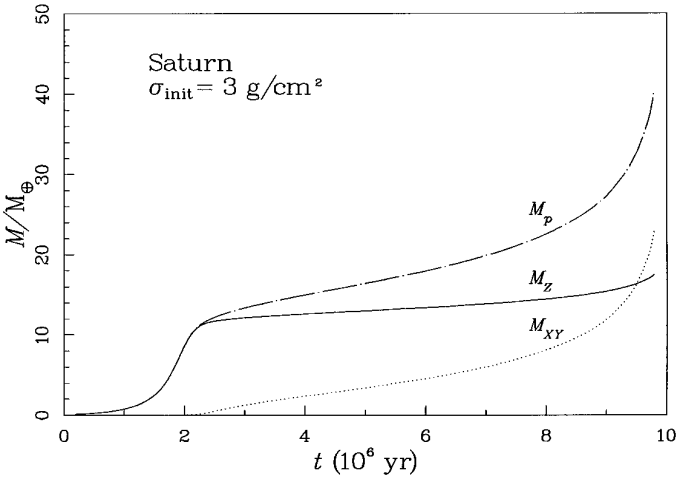

FIG. 4. Cumulative masses (as in Figs. 1a and 2) as a function of time for Saturn model case S1. The duration of phase 2 and the crossover mass M_{cross} are similar to case J1, because the planetary isolation mass and the input physics are similar.

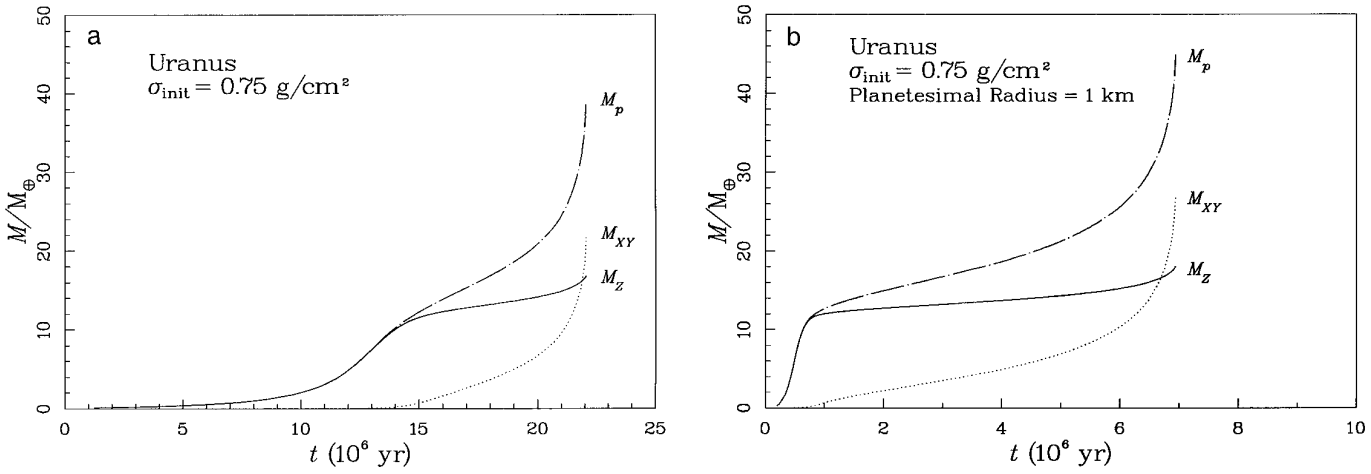

FIG. 5. (a) Cumulative masses (as in Figs. 1a and 2) as a function of time for Uranus case U1. Note the relatively long period during which the model's mass and composition are similar to those of present-day Uranus. (b) Cumulative masses (as in Figs. 1a and 2) as a function of time for Uranus case U2. Note that the decrease in assumed planetesimal size (and the corresponding reduction in planetesimal random velocities) greatly reduces the duration of phase 1.

the nominal Saturn model (9.8×10^6 years) than for the nominal Jupiter model (8.0×10^6 years). This surprising similarity in t_{end} for the nominal Jupiter and Saturn models is because the isolation mass is nearly the same for the two models (see Section 4). Because the isolation masses were chosen to be the same, the value of M_Z at the conclusion of the Saturn simulation ($17.5 M_\oplus$) is close to that for the nominal Jupiter case ($21.5 M_\oplus$).

Case S2 is identical to case S1 except that δ_s is set to zero. As in cases J1 and J4, the lifetime of phase 1 and the value of M_{cross} are hardly affected, but the lifetime of phase 2 is drastically reduced to 1×10^6 years, as compared with 7×10^6 years for case S1. Thus, the Saturn formation time is reduced to only 3.3×10^6 years in this case.

As illustrated by Figs. 2a and b and discussed above, t_{end} depends quite sensitively on σ_{init}. Thus, whether Jupiter or Saturn first reached runaway gas accretion was determined by differences in the actual values of σ_{init} from the ones selected for our nominal models. In principle, we might be able to make rough estimates of these differences if we knew accurately the high-Z masses of these two planets. However, at present there is disagreement as to which planet has the larger M_Z (Zharkov and Gudkova 1991, Chabrier *et al.* 1992).

Figure 5a shows the evolutionary history of the "Uranus" case U1, where $\sigma_{init} = 0.75$ g/cm^2 and $a = 19.2$ AU. Again we simply scaled σ_{init} as a^{-2}. The time scale for phase 1 reaches about 1.5×10^7 years, about a factor of 8 longer than that for Saturn. Again, $M_Z(t_{end}) = 17 M_\oplus$ and $t_{end} = 2.2 \times 10^7$ years, a factor of 2.2 longer than that for Saturn. Note that $M_{XY} = 1.7 M_\oplus$ and $M_Z = 12.4 M_\oplus$, comparable to the present-day Uranus, after 1.6×10^7 years of evolution. The period during which M_{XY} is in the range 1–$4 M_\oplus$ lasts 4 million years, from 15 to 19 myr. In a rerun of the "Uranus" case with small planetesimals (case U2; Fig. 5b) the factor F_g reaches a maximum of 7.5×10^5 during the early phases as compared with a maximum of 1.8×10^4 in case U1. As a result, t_{phl} is drastically shortened by a factor 15, to 1×10^6 years. The time for phase 2, however, is not much affected, lasting 6.7×10^6 and 5.8×10^6 years in cases U1 and U2, respectively. Also, the values for M_{cross} are very similar. However, the time at which $M_{XY} = 1.7 M_\oplus$ in case U2 is only 1.6×10^6 years, a factor of 10 earlier than the comparable time for case U1. The envelope mass stays in the range 1–$4 M_\oplus$ between 1.5×10^6 and 3.5×10^6 years. Thus, a model with characteristics similar to those of the present planet can easily be obtained on time scales $\lesssim t_{neb}$. The parameters for case U2 give a formation time for Uranus that is too short compared with the nominal formation times of Jupiter and Saturn; a slightly smaller value of σ_{init} would improve the fit. Since the planetesimal size has a decisive influence on the time scale for evolution of the model for Uranus, that time scale should be considered very uncertain, and future work should include consideration of a range of planetesimal sizes and the evolution of the size distribution as a result of accretion.

4. DISCUSSION

4.1. Gas Accretion Rate

Here, we try to understand the factors that control the gas accretion rate, especially the conditions that lead to runaway gas accretion (phase 3). Despite differences in absolute scales, all evolutionary models run to date share certain basic characteristics. There are always three phases. These phases are distinguished by the temporal behavior

of the gas and planetesimal accretion rates, the relative magnitudes of these two rates, and the relative magnitudes of the cumulative amounts of accreted low- and high-Z material. We use these properties, in conjunction with the sensitivity of the gas accretion rate to key parameters, to infer the factors that control the rate of gas accretion during each of these phases. For convenience, we use the terms *envelope* and *low-Z mass* interchangeably below, as well as the terms *core* and *high-Z mass*.

In a formal sense, the rate of gas accretion, as determined here, is defined by the new volume of space opened up at the outer edge of the planet's envelope by a combination of the contraction of constant-mass shells near this edge and the expansion of the outer boundary that results from the increase in the protoplanet's total mass. The basic properties of our evolutionary models can be understood in terms of which of these two processes is the dominant one and which component of the accretion controls its rate of change. During phase 1, the envelope's mass is small, and, except near the end, the planetesimal accretion rate is high, always exceeding that of the gas accretion. The planet's mass is increasing rapidly almost solely due to the accretion of planetesimals. However, the rate at which the outer envelope contracts is greater than the rate of expansion of the outer boundary. Therefore, the rate of gas accretion is controlled by the rate at which the envelope contracts, which, in turn, is controlled by the energy supplied by planetesimal accretion. This conclusion is consistent with the fact that M_{XY} is more than twice as large at the end of phase 1 in case J4 than it is in case J1. For Jupiter models with 100-km planetesimals, Eqs. (14) and (15) give $t_{\rm ph1} \propto \sigma_{\rm init}^{-0.5} F_{\rm g}^{-1}$. As the average value of $F_{\rm g}$ increases weakly with $\sigma_{\rm init}$ (because the average mass of the planet is larger), the actual calculations are closer to $t_{\rm ph1} \propto \sigma_{\rm init}^{-1}$.

During phase 2, the envelope's mass is smaller than that of the core, the gas accretion rate exceeds that of planetesimal accretion, and both rates are nearly constant in time and relatively low. This behavior suggests that the rate of gas accretion is determined by $dR_{\rm p}/dt$. The reason is that the high-Z material dominates the total mass, while the added material is mainly gas, so that the planet's total mass, and therefore $R_{\rm bd}$, increases only slowly with time.

To examine the nature of phase 2 more carefully, we reran the baseline case but stopped all planetesimal accretion after certain selected times (1.5, 3.5, and 6.8 myr) during phase 2. These runs are denoted as cases J1a, J1b, and J1c, and the masses and accretion rates are plotted as a function of time in Figs. 6a and b, respectively. The results show that the gas accretion rate (Fig. 6b) jumps suddenly by a factor of about 4 in each case right after planetesimal accretion is halted. This change is a consequence of the energy balance within the planet, as the planet's total luminosity remains the same. The length of the remaining time in phase 2 is reduced to 1.5, 1.0, and 0.25 myr, respectively, in the three cases, corresponding in each case to a factor of 4 shorter than the remaining time in the baseline case.

These calculations, along with the previous cases, help to define the nature of phase 2. Depending of the principal energy source, the length of this phase depends on either the gravitational contraction (Kelvin–Helmholtz) time scale of the envelope or the time scale for accretion of planetesimals. In the first case, the contraction time is given to within a factor of 2 by

$$t_{\rm c} \approx \frac{|E_{\rm grav}|}{L} \sim \frac{GM_{\rm core}M_{\rm env}}{RL}, \tag{19}$$

where $E_{\rm grav}$ is the gravitational energy of the added mass and L is the planet's luminosity. For the baseline case, in the absence of planetesimal accretion, $t_{\rm c} \sim 1$ myr, based on a radius $R = 5 \times 10^{10}$ cm, inside of which ~90% of the envelope mass is contained. This estimate is in agreement with the results of case J1a, where the planetesimal accretion is cut off early in phase 2. The evolution of cases J1b and J1c after cutoff is faster, because less gas remains to be accreted to reach $M_{\rm cross}$. This time scale is also consistent with the phase 2 times of cases J4 (1.3 myr) and S2 (1.0 myr), in which the energy generation rate from planetesimals is sharply reduced compared with the standard case. The luminosity, which is an important factor in the determination of $t_{\rm c}$, depends on internal properties of the model, such as opacity.

As gas is accreted, however, the added mass results in an increased supply of planetesimals in the feeding zone [cf. Eqs. (4) and (7)]. As these accrete onto the protoplanet [Eq. (17)], they generate an accretion luminosity, which for $\delta_{\rm s} = 1$ is given by

$$L_{\rm pl} \approx \frac{GM_{\rm core}\dot{M}_Z}{R_{\rm core}}. \tag{20}$$

The phase 2 luminosities for case J1, J2, and J3 are in good agreement with this expression, given the calculated values of $\dot{M}_Z$. However, $\dot{M}_Z$ itself is determined by other factors. The main physical effect that determines the time scale is the mass–luminosity relation that is intrinsic to the structure of the protoplanet. The energy loss rate through the planet is determined by the rate of radiative transfer, which depends on the opacity. In the case of stars with constant opacity, standard stellar interiors theory gives $L \propto M^3$ (Clayton 1983, p. 185). In the present case, the situation is complicated by the core–envelope structure and by the variation of the opacity with temperature and density. During most of phase 2, where the relevant mass is close to the isolation mass, the numerical results are closer to $L \propto$

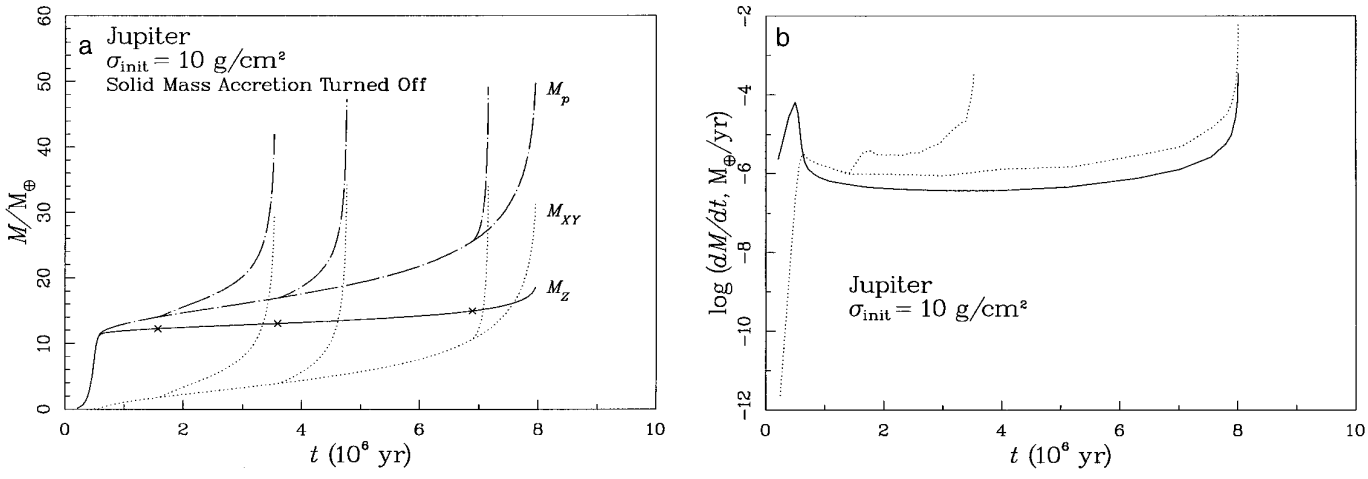

FIG. 6. (a) Cumulative masses (as in Fig. 1a) as a function of time for cases J1a, J1b, and J1c. The curves extending farthest to the right correspond to case J1. The other curves (left to right) show runs in which planetesimal accretion was arbitrarily stopped at times 1.5, 3.5, and 6.8 myr, respectively, with all other parameters the same as in case J1. Crosses show the core mass (M_Z) at these times. (b) Accretion rates as a function of time for case J1 and J1a. The curves extending farthest to the right correspond to case J1. The other curve shows the gas accretion rate in which planetesimal accretion was arbitrarily stopped at time 1.5 myr.

M^n, where $4 \lesssim n \lesssim 5$. In any case, if planetesimal accretion supplies most of the radiated luminosity and all high-Z material sinks to the core (as in these three cases), the time scale is approximately derived as follows: The total energy released during phase 2 is

$$E_{\rm tot} \approx L \times t_{\rm ph2} \approx GM_{\rm core}\frac{\Delta M_Z}{R_{\rm core}}, \qquad (21)$$

where ΔM_Z is the added planetesimal mass during phase 2. [If contraction of the envelope is an important energy source, or dissolved planetesimals do not sink, a relationship similar to (21) holds provided the masses and radius used are adjusted to represent appropriately averaged quantities for the planet.] But $\Delta M_Z \propto M_{\rm iso}$ [cf. Eq. (18)], and $R_{\rm core} \propto M_{\rm core}^{1/3}$, therefore

$$t_{\rm ph2} \propto M_{\rm iso}^{5/3}/L. \qquad (22)$$

Contraction of the planet's envelope determines the thermal energy input for the planet, contributing both directly via the release of gravitational potential energy in the envelope and indirectly because it controls $\dot{M}_{XY}$ and thus, via Eq. (17), $\dot{M}_Z$ and the energy supplied by planetesimal accretion. For example, if the luminosity is low, a slow rate of contraction is required to bring planetesimals in at a sufficient rate to supply this luminosity; therefore, $\dot{M}_Z$ also is low [Eq. (17)] and the time scale is long. To compare with the numerical results, cases J2 and J3 differ in isolation mass by a factor of almost 3. Assuming a mass–luminosity relation with $n = 4\frac{2}{3}$, the duration of phase 2 should go approximately as $M_{\rm iso}^{-3}$, which is reasonably consistent with the factor of 43 difference that is actually obtained in these two cases. Table V shows a comparison between the above estimate for phase 2 time scales (using for definiteness the minimum value of luminosity, $L_{\rm min}$) and the actual numerical results. The similarity of the numerical values of the ratio listed in the final column of Table V for runs J1 and J5–J7 is a consequence of the energy balance; the similarity of the number for runs J2 and J3 supports the scaling given by expression (22). Substantially larger ratios are obtained for runs J4 and J8 because less energy is released by planetesimals if they do not sink to the core, and thus, contraction of the envelope supplies most of the energy for the planet's luminosity, which implies that Eq.

TABLE V[a]

run	$\sigma_{init,Z}$	M_{iso}	L_{min}	$M_{iso}^{5/3}/L_{min}$	t_{ph2}	$M_{iso}^{5/3}/(L_{min}t_{ph2})$
J1	10.0	11.58	7.586×10^{-8}	7.814×10^{8}	6.97	3.554×10^{-6}
J2	7.5	7.52	6.457×10^{-9}	4.471×10^{8}	47.19	3.004×10^{-6}
J3	15.0	21.28	1.318×10^{-6}	1.240×10^{8}	1.06	3.708×10^{-6}
J4	10.0	11.58	1.413×10^{-7}	4.196×10^{8}	1.27	1.048×10^{-5}
J5	10.0	11.58	6.918×10^{-8}	8.567×10^{8}	7.02	3.869×10^{-6}
J6	10.0	11.58	2.512×10^{-7}	2.360×10^{8}	2.20	3.401×10^{-6}
J7	10.0	11.58	7.762×10^{-8}	7.636×10^{8}	6.68	3.624×10^{-6}
J8	10.0	11.58	1.288×10^{-7}	4.601×10^{8}	0.96	1.520×10^{-5}
S1	3.0	11.73	8.511×10^{-8}	7.115×10^{8}	7.02	3.213×10^{-6}
S2	3.0	11.73	1.862×10^{-7}	3.252×10^{8}	1.01	1.021×10^{-5}
U1	0.75	11.92	8.913×10^{-8}	6.979×10^{8}	6.70	3.303×10^{-6}
U2	0.75	11.92	9.772×10^{-8}	6.365×10^{8}	5.77	3.497×10^{-6}

[a] $\sigma_{\rm init,Z}$ is in units of g/cm², $M_{\rm iso}$ is in units of Earth masses, $M_\oplus$, $L_{\rm min}$ is in units of solar luminosity, $L_\odot$, and $t_{\rm ph2}$ is in units of myr.

(19) rather than expression (22) is the primary determining factor for t_{ph2}. Note that if the contraction rate of the planet were to increase suddenly, the rate of accretion of solids would also increase, generating an increased planetesimal accretion luminosity, which would tend to suppress the rapid increase in M_{XY}. Thus, to some extent phase 2 is self-regulating and stable.

In all models presented here, the transition to runaway gas accretion begins when $M_Z \approx 0.8 M_{cross}$ and $M_{XY} \approx 0.2 M_{cross}$; however, for definiteness and for consistency with earlier work, we define the onset of phase 3 at $M_Z = M_{XY} = M_{cross}$. During the transition and during phase 3 itself, the rates of gas and planetesimal accretion both increase in a quasi-exponential fashion with time, but the gas accretion rate grows more rapidly than does the planetesimal accretion rate. Hence, the cumulative amount of low-Z mass in the protoplanet in phase 3 becomes progressively more and more the dominant component [cf. Eqs. (16) and (17), but note that in phase 3 when $\dot{M}_{XY}$ is very large, the accretion rate of planetesimals is unable to keep pace with the expansion of the planet's accretion zone, so Eq. (17) overestimates $\dot{M}_Z$]. This behavior suggests that the gas accretion rate during phase 3 is determined jointly by dR_p/dt and dR_{bd}/dt, with the contraction of R_p being the ultimate controlling factor. During late phase 2 and all of phase 3, there is an unstable relationship between the amount of mass added and the rate at which the envelope contracts that leads directly to the quasi-exponential growth of the gas accretion rate. Once $M_Z \approx M_{XY}$, the subsequent increase in gas mass produces a comparable increase in the protoplanet's total mass, which, in turn, causes a significant increase in R_{bd}. As a result, there is more gas mass added due to dR_{bd}/dt, which, in turn, leads to an increase in dR_p/dt, and so on. During phase 3, the PdV work associated with envelope contraction becomes the dominant term in the protoplanet's energy budget, whereas the energy associated with planetesimal accretion is the dominant term during phase 1 and the largest term during phase 2 in most cases considered. The importance of the various terms in the energy equation for case J1 is shown in Fig. 7. During phase 1 (up to $t = 6.3 \times 10^5$ years), the radiative loss is almost exactly balanced by planetesimal energy deposition, the error is about 2.5%, and the gravitational and internal energy terms are negligible. During most of phase 2 (up to $t \approx 6 \times 10^6$ years) planetesimal deposition still represents about two-thirds of the energy budget while the typical numerical error is 15%. During phase 3, the gravitational energy release dominates, and the energy budget cannot be calculated accurately because a large amount of new gas is added every time step.

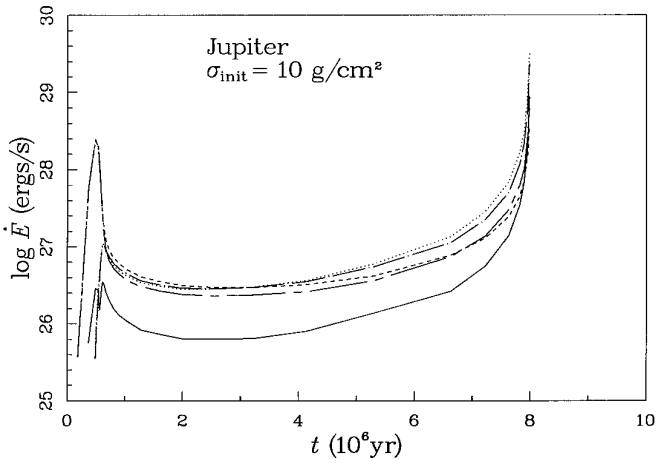

FIG. 7. Global energy budget as a function of time for case J1. The various terms in the energy equation, in erg/sec, are integrated over the entire planetary envelope. Plotted are the radiated luminosity (dashed line), the energy deposition from planetesimals (long- and short-dashed line), the rate of change of internal energy (dotted line), the rate of change of gravitational energy of the envelope (dot–dashed line), and the sum of all contributions (solid line), which indicates the error.

4.2. Comparisons with Other Calculations

In what ways have our simulations shed new light on the formation of the giant planets? What are the key issues that remain to be investigated? In particular, what are the critical parameters, the resulting temporal behavior of the rate of gas accretion, the time scale to reach runaway gas accretion, and the low- and high-Z masses at this point?

The classical static calculations of Mizuno (1980) and the later evolutionary simulations of BP86 were performed for solar composition envelopes, grain-dominated opacity in the outer envelope, and, of greater importance here, a time-invariant rate of planetesimal accretion. The simulations of this paper are distinguished from those of its predecessors chiefly by the explicit calculation of the rate of planetesimal accretion for situations involving isolated, massive protoplanetary embryos surrounded by a swarm of much less massive planetesimals. This choice of accretional environment for the forming giant planets ensures a large time variation in the planetesimal accretion rate, as, in fact, is well demonstrated by the results of our simulations (cf. Figs. 1a, b). Although our choice, therefore, represents an extreme situation, it constitutes one plausible pathway by which the giant planets could have formed on time scales that are consistent with the lifetime of the solar nebula and the age of the Solar System (Lissauer 1987).

In the older simulations, the gas accretion rate increased with time in a quasi-exponential fashion throughout the entirety of the simulation, although its rate of increase became steeper with increasing time. In this sense, there was just one continuous phase of accretion, with the runaway portion simply being marked by the time where the gas accretion rate first exceeds the planetesimal accretion rate. This point lies quite close to that where the low- and high-Z masses equal one another. In the current calcula-

tions, there are three major phases along the evolutionary tracks. During phases 1 and 3, the gas accretion rate increases in a quasi-exponential fashion with time, but it has a nearly constant rate during phase 2. Phase 2 occurs when the planet's feeding zone is almost entirely depleted by previous accretion, and its properties depend strongly on the mutual interactions of the planetesimal and gas accretion rates. More generally, allowance for a time-varying rate of planetesimal accretion leads to both qualitative and quantitative differences between the current calculations and their predecessors.

Runaway gas accretion, however, still begins near the point where the low- and high-Z masses are equal. We suspect that this similarity arises from a common cause: the sensitivity of the gas accretion rate to the location of the planet's outer boundary once the low-Z mass becomes a significant fraction of the planet's total mass. Under these conditions, there is a strong and unstable relationship between the rate of contraction of constant-mass shells in the outer envelope and the rate of expansion of the outer boundary, leading to runaway gas accretion.

Previous calculations (BP86) showed that the crossover mass, $M_{\rm cross}$, was insensitive to the outer boundary parameters $\rho_{\rm neb}$ and $T_{\rm neb}$. In the present calculation, $M_{\rm cross}$ is also insensitive to $\rho_{\rm neb}$ ($T_{\rm neb}$ was not tested). The value that BP86 obtained for $M_{\rm cross}$ was modestly sensitive to the grain opacity, in the sense that it decreased by 27% when the opacity was reduced by a factor of 50. In the present case, a factor of 50 reduction in opacity results in practically no change in $M_{\rm cross}$, which depends almost solely on $M_{\rm iso}$ [Eq. (18)] and, therefore, on $\sigma_{\rm init}$ and a [Eq. (14)], but the time scale to pass through phase 2 is a factor of 3 shorter. In both sets of simulations, the reduction in opacity results in an increase in radiated luminosity by a factor of 3, so the rate of gravitational contraction must speed up, relative to the baseline case, to supply the extra energy. Thus, there is a faster rate of gas accretion from the nebula. In our simulations, this increase in $\dot{M}_{XY}$ leads to an increase in $\dot{M}_Z$ [cf. Eq. (17)] so there is no change in $M_{\rm cross}$, but $t_{\rm cross}$ decreases significantly, whereas $\dot{M}_Z$ is fixed in the simulations of BP86, so that both $M_{\rm cross}$ and $t_{\rm cross}$ decrease with decreasing opacity. The range of values for $M_{\rm cross}$ in BP86 (11–$29 M_\oplus$) is practically the same as the range in the present calculation (10–$30 M_\oplus$). The values of $M_{\rm cross}$ computed by BP86 also depended on the assumed planetesimal accretion rate, $\dot{M}_Z$; a factor of 10 increase in this rate resulted in an increase in $M_{\rm cross}$ by 72%. We find, as before, that a higher $M_{\rm cross}$ is associated with a higher planetesimal accretion rate, corresponding in the present case to a higher $\sigma_{\rm init}$.

In the calculations of BP86, the time scale to reach runaway gas accretion was determined almost entirely by the specified value of $\dot{M}_Z$; these times ranged from 3×10^6 to 1.12×10^8 years. In the current calculations a similarly wide range was found, from 2×10^6 to 5×10^7 years, with a strong dependence on $\sigma_{\rm init}$, a, $\delta_{\rm s}$, and the opacity. This time scale is in most cases determined by the length of phase 2, which was discussed in Section 4.1. For example, for standard Jupiter parameters (cases J1 and J4), a change in $\delta_{\rm s}$ from 1 to 0 resulted in a change in time scale from 8×10^6 to 1.6×10^6 years. Presumably the "truth" lies somewhere inbetween the extremes of $\delta_{\rm s} = 0$ and $\delta_{\rm s} = 1$. Thus, reasonable parameter choices lead to formation times for Jupiter and Saturn of 5×10^6 and 7×10^6 years, respectively. A surprising result of this calculation is the similarity of the phase 2 time scales in the standard models of Jupiter, Saturn, and Uranus (cases J1, S1, U1): they are all 7×10^6 years. This result is a consequence of the same isolation masses being chosen in all three cases, so that the model structures at the end of phase 1, the luminosities, the gravitational contraction times, and the energy deposition by planetesimals in phase 2 were all about the same. In retrospect, this is not surprising, as we have already shown that the duration of phase 2 is not sensitive to the density and temperature of the nebula gas, which are the only other variables involved.

4.3. Implications for the Solar Nebula

Within the context of our model, it is possible to derive tight bounds on the "initial" surface density of planetesimals, $\sigma_{\rm init}$, in the outer Solar System. These bounds come from the joint constraints of time scale and the current high-Z masses of the giant planets. On the one hand, $\sigma_{\rm init}$ needs to be smaller than some upper bound or the model planets would have accreted more high-Z mass than they currently contain. On the other hand, $\sigma_{\rm init}$ needs to be larger than some lower bound or giant planet formation would violate a time scale constraint. This constraint is set by the lifetime of the gas component of the solar nebula, $t_{\rm sn}$, estimated from observations to be $\lesssim 10^7$ years. Jupiter and Saturn need to reach phase 3 and Uranus and Neptune need to reach phase 2 before this time.

We estimate that $\sigma_{\rm init} \approx 10$ g/cm^2 in the region of the solar nebula where Jupiter formed. This value cannot be increased by more than about 50% nor decreased by more than about 20% without violating one of the two constraints cited above. This value is about a factor of 4 larger than that given by the minimum-mass solar nebula of Hayashi *et al.* (1985). It is also about a factor of 2 smaller than that estimated by Lissauer (1987), based on the assumption that Jupiter's core grew to $>15 M_\oplus$ before it became isolated. Our value of $\sigma_{\rm init}$ is somewhat smaller than that of Lissauer because a giant planet can still acquire high-Z mass after nearly depleting its feeding zone at the end of phase 1 by the outward expansion of its feeding zone during phases 2 and 3. As a result, a smaller demand is placed on the fully formed Jupiter to scatter the remaining planetesi-

mals out of the Solar System. Put another way, Jupiter should have moved only a small fraction of its initial distance from the Sun due to this clearing out of planetesimals, as its total mass would have been significantly larger than the cumulative mass of removed planetesimals.

Since the terrestrial planets have relatively low masses and are more deeply embedded in the Sun's gravitational well than is Jupiter, they would not have been able to effectively scatter planetesimals out of the region of the inner Solar System. Thus, σ in the inner Solar System should have been close to the values provided by the minimum-mass solar nebula (e.g., Lissauer 1987). Therefore, σ varied only slowly with distance from the Sun throughout the inner Solar System and out to the distance of Jupiter, aside from a possible discontinuity caused by the condensation of water ice near the vicinity of Jupiter (Lissauer 1987). However, our two basic constraints on σ in the region where the giant planets formed imply that $\sigma \propto a^{-2}$ in the outer solar nebula if the high-Z mass is actually the same for Jupiter and Saturn. Thus, the values of σ given by our simulations tend to approach those of the minimum-mass solar nebula of Hayashi *et al.* (1985) with increasing distance from the Sun; i.e., the enhancement factor was largest for Jupiter.

Our inferred dependence of σ on distance from the Sun in the giant planet region (a^{-2}) is much steeper than that expected for a fully viscously evolved disk (no steeper than $a^{-0.5}$; Ruden and Lin 1986) and is more nearly comparable to the distribution in a disk that has just formed by collapse from a rotating molecular cloud core ($a^{-7/4}$; Cassen and Moosman 1981) or that inferred from the spectral energy distributions of young stars ($a^{-3/2}$; Beckwith *et al.* 1990). This comparison suggests either that little viscous evolution occurred in the outer region of the solar nebula or that the radial evolution of solids became quickly decoupled from that of gases in this region of the solar nebula. By contrast, the relatively flat profile of σ inferred for the inner region of the solar nebula implies just the opposite. The viscous evolution time scale can increase with distance from the Sun (Ruden and Lin 1986), so such a surface density profile may be realistic. *We add the strong caveat that the conclusions drawn here and elsewhere in this paper depend strongly on the validity of the basic assumptions of our simulations: isolated embryos and no systematic radial motions of planetesimals.*

Finally, we examine more carefully the conditions under which our scenario for giant planet formation satisfies current estimates of t_{sn}. Our nominal models of Jupiter and Saturn reach runaway gas accretion on time scales of 8.0×10^6 and 9.8×10^6 years, respectively. We set $\delta_s = 1$ in these simulations; i.e., we assume that vaporized planetesimal material sank to the core interface. The opposite extreme, that of no sinking, shortens the time to reach runaway gas accretion by about a factor of 4 (cf. Fig. 3). This time interval can also be shortened by choosing a slightly larger value of σ_{init}. Thus, it is relatively easy to find models for Jupiter and Saturn that reach phase 3 in a time interval comparable to or less than t_{sn}. Note, however, that these time scales again depend on our basic assumptions. For example, if the planetesimal random velocities were assumed to be large, the time scale for phase 1 could well exceed that for phase 2.

At a time of 1.6×10^7 years, early in phase 2, our nominal model reaches a point where its high- and low-Z masses are comparable to those of present Uranus. With smaller planetesimals this time was reduced to 1.5×10^6 years! Note that δ_s does not have much influence on the time scale in this case. Thus, our formation scenario for Uranus is compatible with current estimates of t_{sn}. Neptune has always been the most difficult planet to form quickly enough because of the steep increase in the formation time scale with increasing distance from the Sun. Comparison of our nominal models of Jupiter, Saturn, and Uranus (cf. Figs. 1a, 4, 5a) indicates that the longevity of phase 1, t_{ph1}, scales roughly as a^2. Since Neptune has high- and low-Z masses comparable to those of Uranus (Zharkov and Gudkova 1991), we expect that this scaling law will give us an approximate formation time for Neptune. Extrapolation of our results suggests that $t_{ph1} \approx 3.7 \times 10^7$ years for Neptune for large (100-km) planetesimals but only 3.7×10^6 years for small (1-km) planetesimals. If accretion was dominated by reasonably small planetesimals, we get a time scale for Neptune that is compatible with t_{sn}. Because phase 2 lasts for a long period, these calculations partially resolve the issue of why Uranus and Neptune have very similar properties. However, the observed similarity between M_Z values of Jupiter, Saturn, Uranus, and Neptune must be considered a consequence of the "initial" distribution of condensed mass within the protoplanetary disk rather than a result of fundamental growth processes of the giant planets.

4.4. Implications for Giant Planets

As illustrated in Fig. 1e, the capture radius for planetesimals starts to significantly exceed the core radius when the accreted mass of high-Z material reaches $\approx 2M_\oplus$. Shortly afterward, at a core mass $M_{dis} \approx 2.6M_\oplus$, planetesimals dissolve in the envelope. The precise value of M_{dis} decreases modestly as the planetesimal size decreases, and it is smaller by a few tens of percent in case S1 as compared with case J1. Overall, its range is $2\text{–}4M_\oplus$. This finding strongly suggests that much of the high-Z mass of the giant planets is located (although not necessarily uniformly distributed) within their envelopes, rather than in a segregated core. This prediction is in good accord with the results of recent interior models (Zharkov and Gudkova 1991, Chabrier *et al.* 1992), which yield interior core masses

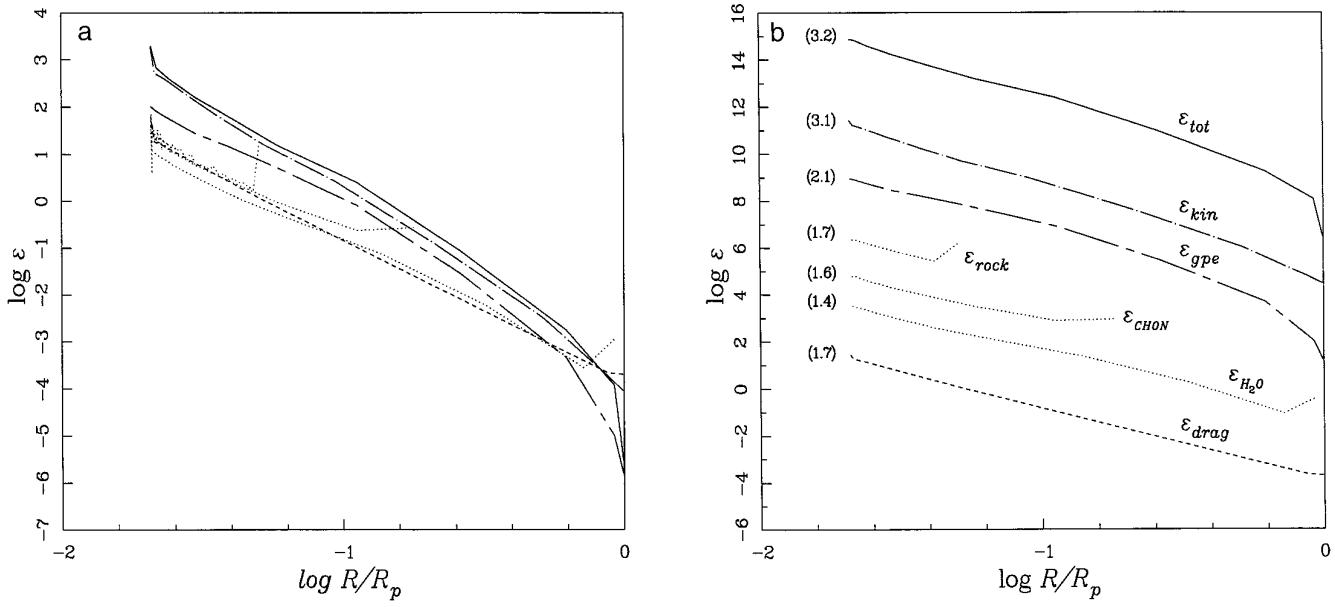

FIG. 8. Rate of energy deposition by planetesimals in the planetary envelope as a function of the distance from the planet's center, R, at a time of 3.5×10^5 years in the evolution of case J1. The planet's radius $R_p = 4 \times 10^{10}$ cm. Energies are given in ergs/g/sec. Plotted are the total energy (solid line), the latent heats (dotted lines) delivered by organics (ε_{CHON}) and absorbed by H_2O and rock, the contribution from gas drag (dashed line), the gravitational potential energy (long- and short-dashed line), and the kinetic energy (dot–dashed line). The core mass is $1.4M_\oplus$ and the envelope mass is 8.6×10^{-6} $M_\oplus$. (a) The curves are overplotted using the same scale. (b) The same curves are displaced vertically by arbitrary amounts for clarity. The number at the upper end of each curve gives the logarithm of the maximum rate of energy deposition in units of erg/g/sec.

in the range 1 to $8M_\oplus$ for Jupiter and Saturn. The core mass could be augmented over M_{dis} by some settling of material to the core or by the occasional accretion of a very massive planetesimal; nevertheless, the ''truth'' probably lies closer to $\delta_s = 0$ than $\delta_s = 1$. This point is illustrated in Figs. 8 and 9, which show where in the protoplanet most of the accretion energy of the planetesimals is deposited. At an early time, during phase 1 when $M_Z = 1M_\oplus$, most of the energy is deposited at the core boundary (Fig. 8), while at a later time during phase 2 much of the energy is deposited at 10 core radii (Fig. 9).

It is likely that some of the dissolved high-Z material ultimately gets mixed throughout the planets' envelopes. The models of the present study have extensive convection zones, similar to those reported by BP86. Furthermore, the calculations of the subsequent evolution (BP86) show that the envelopes become fully convective during their contraction period after accretion has ceased. Thus, another consequence of our simulations is that elements that were derived primarily from the accretion of planetesimals (e.g., carbon) should have abundances in the atmospheres of the giant planets with respect to H that exceed solar. There is good evidence that this is the case (Gautier and Owen 1989). Furthermore, the variation in the degree of enhancement above solar proportions among the four giant planets is qualitatively and semiquantitatively in accord with the expectations of planetesimal dissolution (Pollack *et al.* 1986, Podolak *et al.* 1988, Simonelli *et al.* 1989). Note, however, that the present calculations do not account for the redistribution of heavy elements through the envelope, nor are they carried to the point where the mass approaches that of Jupiter; therefore, a detailed comparison of these results with observations of heavy element abundances in the giant planets is not warranted. Regarding the mixing, a possibly significant factor is the radial gradients in mean molecular weight induced by deposition of heavy elements, an effect that may limit the luminosities of present-day Uranus and Neptune (Hubbard *et al.* 1995). We intend to account for mixing of the heavy elements, including the effect of composition gradients, using more self-consistent calculations in the future.

Zharkov and Gudkova (1991) suggested that the relatively low core masses of Jupiter and Saturn derived from their interior modeling were inconsistent with the critical high-Z masses of $10–15M_\oplus$ predicted by core instability formation models. Therefore, they concluded that Jupiter and Saturn did not obtain their low-Z masses by means of the runaway gas accretion process that occurred once the critical core mass was attained. In the present calculation, all high-Z mass was assumed to end up in the core, although the energy deposition in the envelope was taken into account. Future calculations including mass deposition in the envelope are necessary to test Zharkov and Gudkova's conclusions.

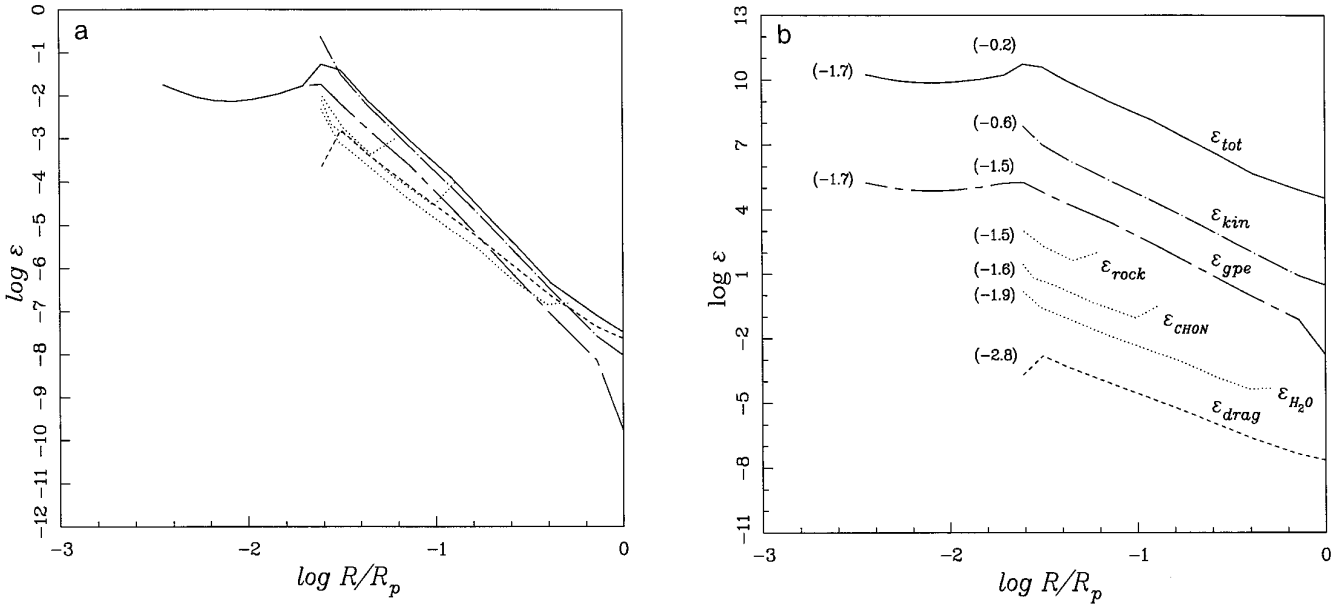

FIG. 9. Same as Fig. 8 except that $t = 4.0 \times 10^6$ years, $R_p = 5.076 \times 10^{11}$, the core mass is $13.2M_\oplus$, and the envelope mass is $4.4M_\oplus$. Note that in this case a larger fraction of planetesimal energy is deposited well above the core because the planetesimals do not reach the core intact.

5. CONCLUSIONS

In the evolution of a giant planet, allowance for a variable rate of planetesimal accretion ($\dot{M}_Z$) results in an important qualitative difference from the case in which $\dot{M}_Z$ is assumed to be constant. In the case of constant $\dot{M}_Z$, there are two phases. In the first phase, $\dot{M}_Z$ dominates the energy generation and $\dot{M}_Z > \dot{M}_{XY}$. In the second phase, $\dot{M}_Z < \dot{M}_{XY}$, rapid gas accretion occurs, and gravitational contraction dominates the energy production. In the new scenario, there are three phases. In the first, $\dot{M}_Z$ dominates the energy production and increases rapidly to a maximum, then declines as the isolation mass is reached. In the second, $M_Z > M_{XY}$, $\dot{M}_Z$ declines to a low and nearly constant level, $\dot{M}_{XY} \approx 2$–$4\dot{M}_Z$, but $\dot{M}_Z$ still dominates the energy production. The third phase is analogous to the second phase of the previous scenario (BP86) with constant $\dot{M}_Z$ and sets in, by definition, when $M_Z = M_{XY} = M_{\rm cross}$. Most of the evolution is generally spent in phase 2. Our results suggest a plausible "pathway" by which Jupiter and Saturn could reach phase 3 and undergo rapid gas accretion after a total elapsed time of a few million years, shorter than the lifetime of a solar nebula. We can explain the inferred bulk composition of Uranus and Neptune as the result of the dissipation of the gas component of the solar nebula while the planets were still in the long-lived phase 2, with still relatively small M_{XY}. Our simulations have also confirmed that a key condition for the inception of runaway gas accretion in the parameter regime explored is that the mass of the low-Z envelope is a substantial fraction of the high-Z core. The feedback process responsible for the runaway is the coupling of the contraction of the material of the envelope and the expansion of the outer boundary of the envelope (the accretion radius) with $\dot{M}_{XY}$. Finally, the results of our simulations, which take into account the dissolution of planetesimals in the gaseous envelope, are consistent with the partitioning of high-Z mass between the core and the envelope in the current giant planets and with the supersolar abundance ratios of planetesimal-derived elements in the atmospheres.

The actual rate at which the giant planets accreted small planetesimals is probably intermediate between the constant rates assumed in most previous studies and the highly variable rates found in the present study. The main assumptions in the accretion model are (1) an isolated embryo, (2) an initial phase of runaway accretion of solids, (3) small random velocities and sizes of planetesimals, and (4) no planetesimal migration into or out of the current feeding zone. Given this model, the simulations provide strong and interesting constraints on the initial surface density of planetesimals in the outer solar nebula; for our standard parameters we find that $\sigma_{\rm Jupiter} \approx 10$ g cm^{-2}, $\sigma_{\rm Saturn} \approx 3$ g cm^{-2}, and $\sigma_{\rm Uranus} \approx 0.75$ g cm^{-2}. The corresponding formation times (assuming a planetesimal radius = 100 km) are 8×10^6, 1×10^7, and 1.6×10^7 years. The high-Z masses and the evolutionary times are extremely sensitive to $\sigma_{\rm init}$. In our opinion, these constraints should not be taken too literally, given the specific set of assumptions under which the calculations were performed. The above formation times should be regarded as conservatively long. For exam-

ple, if our assumption that all accreted high-Z material eventually falls to the core is relaxed, and material is allowed to remain in the envelope ($\delta_s = 0$), formation times for the giant planets can be reduced to 3×10^6 and 3.5×10^6 years for Jupiter and Saturn, respectively. In the case of Uranus, the formation time is dominated by the length of phase 1 rather than phase 2, and δ_s has little effect. If, however, the assumed planetesimal size is reduced by a factor of 100, the time for the formation of Uranus is reduced by a factor of 10, but the times for Jupiter and Saturn are little affected. Or σ_{init} could be increased slightly, resulting in reduced formation times for all planets, but it cannot be increased by more than $\approx 50\%$; otherwise, the high-Z masses become unacceptably large. On the other hand, allowing for planetesimal migration will slow growth rates for fixed M_Z total, as more planetesimals are accreted at later epochs. There is a strong need to perform follow-up calculations in which (1) alternative planetesimal accretion scenarios are examined, such as the allowance for stirring by nearby competing embryos, (2) the impact of dissolved planetesimal material on the properties of the envelope, such as the opacity and convective instability, are investigated, (3) the effect of occasional impacts of very massive planetesimals are assessed, and (4) hydrodynamic effects in the envelope evolution are examined.

ACKNOWLEDGMENTS

This work was supported by grants from NASA's Planetary Atmosphere Office at UCSC through Cooperative Agreement NCC2-5044 and Joint Research Interchange NCA2-803 with the NASA–Ames University Consortium and by NASA Grants NAGW-1107 and NAGW-3165 at SUNYSB. We thank Kevin Zahnle for his encouragement and numerous comments on the manuscript. We also thank Robert Haberle for allowing us to use his workstation to compute the models and Howard Houben for systems help.

REFERENCES

Alexander, D. R. 1975. Low-temperature Rosseland opacity tables. *Astrophys. J. Suppl.* **29,** 363–374.

Alexander, D. R., and J. W. Ferguson 1994. Low-temperature Rosseland opacities. *Astrophys. J.* **437,** 879–891.

Alexander, D. R., H. R. Johnson, and R. L. Rypma 1983. Effect of molecules and grains on Rosseland mean opacities. *Astrophys. J.* **272,** 773–780.

Beckwith, S. W. V., A. I. Sargent, R. Chini, and R. Güsten 1990. A survey for circumstellar disks around young stars. *Astron. J.* **99,** 924–945.

Bodenheimer, P., and J. B. Pollack 1986. Calculations of the accretion and evolution of giant planets: The effects of solid cores. *Icarus* **67,** 391–408. (Referred to as BP86 in text.)

Cassen, P. M., and A. Moosman 1981. On the formation of protostellar disks. *Icarus* **48,** 353–376.

Chabrier, G., D. Saumon, W. B. Hubbard, and J. I. Lunine 1992. The molecular–metallic transition of hydrogen and the structure of Jupiter and Saturn. *Astrophys. J.* **391,** 817–826.

Clayton, D. D. 1983. *Principles of Stellar Evolution and Nucleosynthesis.* Univ. of Chicago Press, Chicago.

Cox, A. N., and J. N. Stewart 1970. Rosseland opacity tables for population I compositions. *Astrophys. J. Suppl.* **19,** 243–259.

Gautier, D., and T. Owen 1989. The composition of outer planet atmospheres. In *Origin and Evolution of Planetary and Satellite Atmospheres* (S. K. Atreya, J. B. Pollack, and M. S. Matthews, Eds.), pp. 487–512. Univ. of Arizona Press, Tucson.

Graboske, H. C., Jr., R. J. Olness, and A. S. Grossman 1975. Thermodynamics of dense hydrogen–helium fluids. *Astrophys. J.* **199,** 255–264.

Greenberg, R., J. F. Wacker, W. K. Hartmann, and C. R. Chapman 1978. Planetesimals to planets: Numerical simulations of collisional evolution. *Icarus* **35,** 1–26.

Greenberg, R., S. J. Weidenschilling, C. R. Chapman, and D. R. Davis 1984. From icy planetesimals to outer planets and comets. *Icarus* **59,** 87–113.

Greenzweig, Y. 1991. *Accretion Rates of Protoplanets.* Ph.D. thesis, Department of Physics, University of California at Santa Barbara.

Greenzweig, Y., and J. J. Lissauer 1990. Accretion rates of protoplanets. *Icarus* **87,** 40–77.

Greenzweig, Y., and J. J. Lissauer 1992. Accretion rates of protoplanets: II. Gaussian distributions of planetesimal velocities. *Icarus* **100,** 440–463.

Grossman, A. S., J. B. Pollack, R. T. Reynolds, A. L. Summers, and H. C. Graboske, Jr. 1980. The effect of dense cores on the structure and evolution of Jupiter and Saturn. *Icarus* **42,** 358–379.

Hayashi, C., K. Nakazawa, and Y. Nakagawa 1985. Formation of the Solar System. In *Protostars and Planets II* (D. C. Black and M. S. Matthews, Eds.), pp. 1100–1154. Univ. of Arizona Press, Tucson.

Hubbard, W. B., M. Podolak, and D. J. Stevenson 1995. The interior of Neptune. In *Neptune and Triton* (D. Cruikshank, Ed.), pp. 109–138. Univ. of Arizona Press, Tucson.

Kary, D. M., and J. J. Lissauer 1994. Numerical simulations of planetary growth. In *Numerical Simulations in Astrophysics, Modelling the Dynamics of the Universe* (J. Franco, S. Lizano, L. Aguilar, and E. Daltabuit, Eds.), pp. 364–373. Cambridge Univ. Press, Cambridge.

Jessberger, E. K., J. Kissel, and J. Rahe 1989. The composition of comets. In *Origin and Evolution of Planetary and Satellite Atmospheres* (S. K. Atreya, J. B. Pollack, and M. S. Matthews, Eds.), pp. 167–191. Univ. of Arizona Press, Tucson.

Levin, B. J. 1978. Relative velocities of planetesimals and the early accumulation of planets. *Moon Planets* **19,** 289–296.

Lin, D. N. C., and J. C. B. Papaloizou 1993. On the tidal interaction between protostellar disks and companions. In *Protostars and Planets III* (E. H. Levy and J. I. Lunine, Eds.), pp. 749–835. Univ. of Arizona Press, Tucson.

Lissauer, J. J. 1987. Timescales for planetary accretion and the structure of the protoplanetary disk. *Icarus* **69,** 249–265.

Lissauer, J. J. 1993. Planet formation. *Annu. Rev. Astron. Astrophys.* **31,** 129–174.

Lissauer, J. J., J. B. Pollack, G. W. Wetherill, and D. J. Stevenson 1995. Formation of the Neptune system. In *Neptune and Triton* (D. Cruikshank, Ed.), pp. 37–108. Univ. of Arizona Press, Tucson.

Lissauer, J. J. and C. R. Stewart 1993. Growth of planets from planetesimals. In *Protostars and Planets III* (E. H. Levy and J. I. Lunine, Eds.), pp. 1061–1088. Univ. of Arizona Press, Tucson.

Mazets, E. P., and 14 Colleagues 1987. Dust in Comet p/Halley from Vega observations. *Astron. Astrophys.* **187,** 699–706.

McDonnell, J. A. M., and 27 Colleagues 1987. The dust distribution within the inner coma of Comet p/Halley 1982i: Encounter by Giotto's impact detectors. *Astron. Astrophys.* **187,** 719–741.

Mizuno, H. 1980. Formation of the giant planets. *Prog. Theor. Phys.* **64,** 544–557.

Mizuno, H., K. Nakazawa, and C. Hayashi 1978. Instability of gaseous envelope surrounding planetary core and formation of giant planets. *Prog. Theor. Phys.* **60,** 699–710.

Podolak, M., W. B. Hubbard, and J. B. Pollack 1993. Gaseous accretion and the formation of giant planets. In *Protostars and Planets III* (E. H. Levy and J. I. Lunine, Eds.), pp. 1109–1147. Univ. of Arizona Press, Tucson.

Podolak, M., J. B. Pollack, and R. T. Reynolds 1988. Interactions of planetesimals with protoplanetary atmospheres. *Icarus* **73,** 163–179.

Pollack, J. B., and P. Bodenheimer 1989. Theories of the origin and evolution of the giant planets. In *Origin and Evolution of Planetary and Satellite Atmospheres* (S. K. Atreya, J. B. Pollack, and M. S. Matthews, Eds.), pp. 564–604. Univ. of Arizona Press, Tucson.

Pollack, J. B., D. Hollenbach, S. Beckwith, D. P. Simonelli, T. Roush, and W. Fong 1994. Composition and radiative properties of grains in molecular clouds and accretion disks. *Astrophys. J.* **421,** 615–639.

Pollack, J. B., M. Podolak, P. Bodenheimer, and B. Christofferson 1986. Planetesimal dissolution in the envelopes of the forming giant planets. *Icarus* **67,** 409–443.

Ruden, S., and D. N. C. Lin 1986. The global evolution of the primordial solar nebula. *Astrophys. J.* **308,** 883–901.

Safronov, V. S. 1969. *Evolution of the Protoplanetary Cloud and Formation of the Earth and Planets.* Nauka, Moscow. English translation: NASA TTF-677. 1972.

Simonelli, D. P., J. B. Pollack, C. P. McKay, R. T. Reynolds, and A. L. Summers 1989. The carbon budget in the outer solar nebula. *Icarus* **82,** 1–35.

Stevenson, D. J. 1982. Formation of the giant planets. *Planet. Space Sci.* **30,** 755–764.

Stevenson, D. J. 1984. On forming the giant planets quickly (superganymedean puffballs). *Proc. Lunar Planet. Sci. Conf. 15th,* 822–823.

Strom, S. E., S. Edwards, and M. F. Skrutskie 1993. Evolutionary time scales for circumstellar disks. In *Protostars and Planets III* (E. H. Levy and J. I. Lunine, Eds.), pp. 837–866. Univ. of Arizona Press, Tucson.

Weidenschilling, S. J. 1977. The distribution of mass in the planetary systems and solar nebula. *Astrophys. Space Sci.* **51,** 153–158.

Wetherill, G. W., and G. R. Stewart 1989. Accumulation of a swarm of small planetesimals. *Icarus* **77,** 330–357.

Wuchterl, G. 1991. Hydrodynamics of giant planet formation: III. Jupiter's nucleated instability. *Icarus* **91,** 53–64.

Wuchterl, G. 1995. Giant planet formation. In *Comparative Planetology* (M. T. Chahine, M. F. A'Hearn, and J. Rahe, Eds.). Dordrecht, Kluwer, in press.

Zharkov, V. N., and T. V. Gudkova 1991. Models of giant planets with a variable ratio of ice to rock. *Ann. Geophys.* **9,** 357–366.